

An evaluation of new particle formation events in Helsinki during a Baltic Sea cyanobacterial summer bloom

Roseline C. Thakur¹, Lubna Dada^{1,2,3}, Lisa J. Beck¹, Lauriane L.J. Quéléver¹, Tommy Chan¹, Marjan Marbouti^{1,11}, Xu-Cheng He¹, Carlton Xavier¹, Juha Sulo¹, Janne Lampilahti¹, Markus Lampimäki¹, Yee Jun Tham^{1,10}, Nina Sarnela¹, Katrianne Lehtipalo^{1,4}, Alf Norkko^{7,8}, Markku Kulmala^{1,5,6}, Mikko Sipilä¹, Tuija Jokinen^{1,9}

¹Institute for Atmospheric and Earth System Research/Physics, Faculty of Science, 00014 University of Helsinki, Helsinki, Finland.

²School of Architecture, Civil and Environmental Engineering, École Polytechnique Fédérale de Lausanne, Lausanne, Switzerland.

³Laboratory of Atmospheric Chemistry, Paul Scherrer Institute, 5232 Villigen PSI, Switzerland

⁴Finnish Meteorological Institute, Helsinki, Finland.

⁵Aerosol and Haze Laboratory, Beijing Advanced Innovation Center for Soft Matter Science and Engineering, Beijing University of Chemical Technology, 100089 Beijing, China.

⁶Joint International Research Laboratory of Atmospheric and Earth System Sciences, Nanjing University, 210023 Nanjing, China.

⁷Tvärminne Zoological Station, University of Helsinki, J.A. Palméns väg 260, FI-10900 Hangö, Finland.

⁸Baltic Sea Centre, Stockholm University, Stockholm, Sweden.

⁹Climate & Atmosphere Research Centre (CARE-C), The Cyprus Institute, P.O. Box 27456, Nicosia, CY-1645, Cyprus.

¹⁰School of Marine Sciences, Sun Yat-Sen University, Zhuhai 519082, China.

¹¹Department of Electronics and Nano-engineering, Aalto University, 00076 Aalto, Finland.

Correspondence to: roseline.thakur@helsinki.fi

Abstract

Several studies have investigated New Particle Formation (NPF) events from various sites ranging from pristine locations, including forest sites to urban areas. However, there is still a dearth of studies investigating NPF processes and subsequent aerosol growth in coastal yet semi-urban sites, where the tropospheric layer is a concoction of biogenic and anthropogenic gases and particles. The investigation of factors leading to NPF becomes extremely complex due to the highly dynamic meteorological conditions at the coastline especially when combined with both continental and oceanic weather conditions. Herein, we engage a comprehensive study of particle number size distributions and aerosol-forming precursor vapors at the coastal semi-urban site in Helsinki, Finland. The measurement period, 25 June 2019–18 August 2019, was timed with the recurring cyanobacterial summer bloom in the Baltic Sea region and coastal regions of Finland. Our study recorded several regional/local NPF and aerosol burst events during this period. Although the overall anthropogenic influence on sulfuric acid (SA) concentrations was low during the measurement period, we observed that the regional or local NPF events, characterized by SA concentrations in the order of 10^7

43 molecules per cm^{-3} occurred mostly when the air mass travelled over the land areas. Interestingly,
44 when the air mass travelled over the Baltic Sea, an area enriched with algae and cyanobacterial
45 blooms, high iodic acid (IA) concentration coincided with an aerosol burst or a spike event at the
46 measurement site. Further, SA-rich bursts were seen when the air mass travelled over the Gulf of
47 Bothnia, enriched with cyanobacterial blooms. The two most important factors affecting aerosol
48 precursor vapor concentrations, and thus the aerosol formation, were speculated to be (1) the type of
49 phytoplankton species and intensity of bloom present in the coastal regions of Finland/ Baltic Sea and
50 (2) the wind direction. During the events, most of the growth of sub-3 nm particles was probably due
51 to SA, rather than IA or MSA, however much of the particle growth remained unexplained indicative
52 of the strong role of organics in the growth of particles, especially in the 3–7 nm particle size range.
53 Further studies are needed to explore the role of organics in NPF events and the potential influence
54 of cyanobacterial blooms in coastal locations.

55

56 Keywords: coastal environment, particle growth, methane sulfonic acid, cyanobacterial summer
57 bloom, sulfuric acid, iodic acid.

58

59 **1 Introduction**

60 New particle formation (NPF) and growth of aerosols are regional processes occurring globally
61 introducing a substantial aerosol load into the atmosphere. NPF has been observed in different
62 environments, including pristine (Asmi et al., 2016; Jang et al., 2019; Jokinen et al., 2018), polluted
63 boundary layers and urban areas (Kulmala et al., 2021; Kulmala et al., 2017; Manninen et al., 2010;
64 Kulmala et al., 2016; Wang et al., 2017; Cai and Jiang, 2017; Deng et al., 2020; Yao et al., 2018; Du
65 et al., 2021; Yan et al., 2021), boreal forests (Buenrostro Mazon et al., 2016; Dada et al., 2017;
66 Kulmala et al., 2013; Kyrö et al., 2014; Leino et al., 2016; Nieminen et al., 2014; Rose et al., 2018),
67 tropical forests (Artaxo et al., 2013; Wimmer et al., 2018) and mountain tops (Bianchi et al., 2016,
68 2020). Few studies have investigated NPF processes in a coastal environment although the coastal
69 NPF research started quite early. The investigation of coastal aerosol events dates back to 1978, when
70 the measurements of total aerosol number concentration were carried out at the Tasmanian coast
71 (Bigg and Turvey, 1978). After that atmospheric nucleation was observed in the Southern hemisphere
72 around the Antarctic coastline (O'Dowd et al., 1997), in Mace Head (Flanagan et al., 2005; McFiggans
73 et al., 2004; O'Dowd et al., 2002), in coastal regions of China and Spain (Yu et al., 2019; Mc Figgans
74 et al., 2010; Mahajan et al., 2011) and in open water regions of North East Greenland (Dall'Osto et
75 al., 2018). Most of these studies have identified biogenic emissions from marine algae as the main
76 precursors driving the new particle formation in a perfect coastal setting.

77 The measurements of gaseous precursors, meteorology and biogenic influences are
78 important to study the coastal NPF, which may lead to the formation of coastal/marine clouds. Coastal
79 clouds are the drivers of many coastal ecosystem (Carbone et al., 2013, Emery et al., 2018, Lawson
80 et al., 2018). Any impact or fluctuations in the cloud formation may impact several other processes
81 of the fragile coastal ecosystem. These coastal clouds demonstrate a high sensitivity to CCN (He et
82 al., 2021) and they have a significant impact on the radiation budget because they have a high infrared
83 emission and albedo when compared to the dark water bodies down below. In this study we highlight
84 the type of NPF processes and their drivers in a semi-urban-coastal setting where the atmosphere
85 could be a mixture of anthropogenic and biogenic emissions. Unlike the above mentioned previous
86 studies which were mostly carried out in a perfect coastal environments where NPF would be most
87 likely affected by the biogenic emissions, this study helps to evaluate the impact of urban emissions
88 Vs coastal emissions on NPF and at large the cloud formation processes.

89 It is well documented that sulfuric acid (henceforth SA) is an important precursor to
90 NPF in most environments (Almeida et al., 2013; Kulmala et al., 2013; Croft et al., 2016; Jokinen et
91 al., 2017; Kirkby et al., 2011; Sipilä et al., 2010). The advancement in aerosol research, revealed that
92 a binary system of SA and water is not sufficient to produce particles in ambient atmospheric
93 conditions without stabilizing compounds (Benson et al., 2008; Duplissy et al., 2016; Kirkby et al.,
94 2011). More recently, it has been found that a ternary system involving SA-ammonia-water or SA-
95 amines-water yield much higher nucleation rates as compared to the binary system (Kulmala et al.,
96 2000; Benson et al., 2008; Almeida et al., 2013; Glasoe et al., 2015; Kürten et al., 2016). In addition
97 to these systems, organic compounds which are highly oxygenated - thus less volatile- have been
98 found to contribute to secondary organic aerosol (SOA) mass in forested areas, mountain tops and
99 anthropogenically influenced field sites (Ehn et al., 2014; Pierce et al., 2011; Riipinen et al., 2012;
100 Zhang et al., 2009; Heikkinen et al. 2020; et al., 2020) and laboratory experiments have shown that
101 they can contribute also to the first steps of NPF (Simon et al., 2020; Lehtipalo et al., 2018; Kirkby
102 et al., 2016; Tröstl et al., 2016) .

103 Furthermore, another important molecular class, iodine as well as its related oxidized
104 species play a crucial role in NPF especially in coastal areas (Allan et al., 2015; Mahajan et al., 2009;
105 Raso et al., 2017; Sipilä et al., 2016) and in pristine marine locations (Baccarini et al., 2020; Beck et
106 al., 2021; He et al., 2021). Some previous studies have reported the emissions of I₂ from the
107 macroalgae at coastal sites (Huang et al., 2010; Peters et al., 2005; Saiz-Lopez and Plane, 2004).
108 Several studies from coastal sites like Roscoff, France (Mahajan et al., 2009; McFiggans et al., 2010),
109 Mace Head, Ireland (O'Dowd et al., 2002) and other European coastlines (Mahajan et al., 2011; Saiz-
110 Lopez et al., 2012) have reported iodine species initiating NPF. The reported events can be considered

111 as aerosol burst events with high aerosol concentration and having exceptionally high initial growth
112 rates (GR) (O'Dowd et al., 2002; McFiggans et al., 2004; Mahajan, et al., 2011). The study from the
113 Roscoff coast suggests that the daytime emissions of I₂ produced by macroalgae during low tides
114 drives the particle formation (McFiggans et al., 2010). The iodine oxides and/or oxoacids formed by
115 the biogenic emissions from the micro and macroalgae near the coastal regions are capable of self-
116 clustering, which could form new particles with a diameter <3 nm and sometimes with a high gas
117 concentration reaching up to 10⁶ cm⁻³ or even more. Recent studies have shown that ion-induced IA
118 nucleation proceeds at the kinetic limit and the overall nucleation rates (ion-induced nucleation +
119 neutral nucleation) driven by iodine oxoacids (IA and iodic acid, HIO₂) are high, even exceeding
120 the rates of well-known precursors of NPF (He et al., 2021b, 2021a): SA with roughly 100 pptv
121 ammonia under similar conditions (Sipilä et al., 2010). The rapid photolysis of I₂, (< 10 s), produces
122 I atoms above the ocean surface and can be detected in high concentrations close to the source region
123 (McFiggans et al., 2010). However, the compounds with longer lifetimes such as CH₃I (two days)
124 provide a source of iodine throughout the troposphere (Saiz-Lopez et al. 2012).

125 Dimethyl sulfide (DMS) oxidation by OH radical in the daytime and by nitrate radical
126 in the nighttime yields other aerosol precursor gases, such as methane sulfonic acid (henceforth,
127 MSA) and SA (Barnes et al., 2006), which play a crucial role in the NPF processes. In a marine
128 coastal environment, MSA concentrations, which are typically lower than those of SA, could be as
129 low as 10% of SA concentration and could maximally reach 100% of SA concentration (Eisele and
130 Tanner, 1993), yet MSA is a potential candidate to participate in the atmospheric nucleation and
131 growth processes (Beck et al., 2021). The stability of heterogeneous MSA clusters have been studied
132 in laboratory and modelling studies (Chen et al., 2020, 2016, 2015) but no study has yet documented
133 MSA clusters in the field. The limited NPF studies in the semi-urban coastal regions and the dynamic
134 coastal meteorology drives the motivation of this research. Another motivation for this research is
135 that, till date no detailed studies on the impact of biogenic emissions on NPF events in Finland were
136 done before, despite the fact that extensive cyanobacteria blooms occur every year in the Baltic Sea
137 region and neighboring water bodies (including Finnish lakes) (Kahru and Elmgren 2014), which
138 could be a significant source of iodine species, SA and MSA. Increasing temperatures and the
139 excessive nutrient load in the Baltic Sea promote algal growth (Kuosa et al., 2017; Suikkanen et al.,
140 2007, 2013). According to HELCOM (Baltic Marine Environment Protection Commission), the
141 Baltic Sea has warmed 0.3° C per decade, however after 1990 significantly faster at 0.6° C per decade
142 and in Finnish coastal areas the warming is even faster with a 2° C increase since 1990 (Humborg et
143 al. 2019). The amount of blue-green algae (i.e. cyanobacteria) has shown a statistically significant
144 increase in open sea areas in the Gulf of Finland, Sea of Åland and the Sea of Bothnia in the last 40

145 years (Kahru and Elmgren, 2014). The increase in frequency and intensity of cyanobacterial blooms
146 would increase the potential emission of biogenic gases changing the composition of the overlying
147 atmosphere and the atmosphere of the neighboring sites, depending on the meteorological conditions.
148 In this semi-urban coastal setting the concentration of gaseous precursors and aerosol size distribution
149 may be influenced by the local meteorological parameters such as wind direction, wind speed, air
150 mass turbulences especially at the surface layer of the lower atmosphere. Coastal locations are
151 dynamic environments with rapid changes in meteorological parameters, also making the study of
152 NPF more challenging.

153 In this study, we aim at a thorough evaluation of aerosol precursor molecules with a
154 detailed analysis of NPF events during the cyanobacterial bloom period, in the coastal city of
155 Helsinki, Finland, from June to August (summer) 2019. This work evaluates the role of phytoplankton
156 blooms and meteorological parameters in the NPF events observed during the measurement period.
157 We also identify the major precursor vapors and molecular clusters found during the aerosol events.
158 Here, we formulate the hypothesis that gaseous precursors formed from the biogenic emissions from
159 the surrounding marine areas could play an important role in the nucleation processes in Helsinki.
160 Although Helsinki is a coastal area yet the role of marine emissions on NPF processes has not been
161 studied before.

162

163 **2 Measurement Site and Methodology**

164 The measurement sites are surrounded by coastal water bodies (<4km, Vanhankaupunginselkä),
165 forests (<3km) and road connecting to the main city (<300m) as seen in figure 1. Overall Helsinki is
166 located on a relatively flat land on the coast of the Gulf of Finland. The Helsinki Metropolitan area is
167 about 765 km² with approximately one million inhabitants, counting together the city of Helsinki and
168 the neighboring cities of Espoo, Vantaa, and Kauniainen. The climate in southern Finland can be
169 classified as either marine or continental depending on the air-flows and pressure systems. Either
170 way, the weather is milder than typically at the same latitude (60°N) mainly due to the Atlantic Ocean
171 and the warm Gulf Stream.

172



173
 174 **Figure 1:** Map showing the two locations included in the study where instruments were operated
 175 (upper left panel). The yellow polygons on the left side of the measurement locations (on the lower
 176 right panel) show forest/park with little or no traffic (West and Northwest, 300 m from the
 177 measurement site). The yellow double lines on the right of the measurement locations is the traffic
 178 area or the main road (E75) leading to the Helsinki city center (250 m east of the measurement site).
 179 The blue lines depict the coastline after which the lakes and coastal waters of Gulf of Finland start (1
 180 km to the east from the measurement site) © Google Earth 2019.

181
 182 The site and measurement period (25 June 2019–18 August 2019) selected for this particular study
 183 are unique since this semi-urban location could be influenced by emissions from the recurring
 184 summertime blooms in the Baltic sea and the neighboring coastal regions. As per the SYKE press
 185 release (2019) the northern part of the Baltic Sea’s main basin, entrance to the Gulf of Finland and
 186 south of the Åland Islands, were enriched with blue-green algae (cyanobacteria). The bloom lasted
 187 from June-August 2019. In coastal areas, bloom was mostly spotted in the Archipelago Sea, Gulf of
 188 Finland, Bothnian Sea and the Quark. The bloom situation developed rapidly and spatially highly
 189 variable, even over short distances. The fragmented nature of the coastal areas and changing wind
 190 and water currents makes the algal bloom conditions highly dynamic.

191 **2.2 Main Instruments**

192 To understand the chemical composition of the precursor vapors emitted from various sources around
 193 the site, the Chemical ionization Atmospheric Pressure interface-Time Of Flight mass spectrometer

194 (CI-APiTOF) was operated from the 4th floor laboratory of the Physicum building, Kumpula campus,
195 University of Helsinki (60° 12' N, 24° 58' E ; 49m , a.m.sl). The other aerosol and trace gases
196 instruments were operated at the SMEAR III (Station for Measuring Ecosystem-Atmosphere
197 Relation, 60.20° N, 24.96° E; 25 m a.m.s.l.) which is 180 m away from the mass spectrometric
198 measurement site.

199 The Atmospheric Pressure interface-Time Of Flight (APiTOF) mass spectrometer is the
200 state-of-the-art instrument for gas phase chemical composition investigations including aerosol
201 precursor characterizations. Here the instrument is coupled with a nitrate based-chemical ionization
202 (CI) inlet in order to measure neutral gas-phase molecules that are clustered and charged with a
203 reagent ion. In our study we used inlet design as described by Eisele and Tanner (1993) and Kurten
204 et al. (2011) and further used by Jokinen et al., 2012. The Time Of Flight (TOF) mass analyzer can
205 detect molecules with masses up to 2000 Th with a mass resolution of 3600 Th/Th. More details on
206 the working principle of the instrument and calibrations can be found in earlier studies (Junninen et
207 al., 2010, Jokinen et al., 2012; Kürten et al., 2014). The sampled air was drawn in through a 1 m-long,
208 “3/4” diameter stainless steel tube with an average flow rate of 10 Lpm. In this study, the chemical
209 ionization was done via nitrate ions (NO₃⁻) through x-ray exposure of nitric acid (HNO₃, flow rate: 3
210 mLpm), saturating the sheath air flow entering the CI (flow rate: 30 Lpm), the inlet flow of 10 Lpm
211 was reached by using a 40 Lpm total flow. The instrument was calibrated prior to the experiment
212 according to (Kürten et al., 2012) resulting in a calibration factor of 1.45×10^9 molecule per
213 normalized unit signal including the diffusion losses in the inlet line.

214 The resulting data (i.e. obtained signals) were averaged to 60 min before the mass
215 calibration step performed through the MATLAB based program tofTools (Junninen et al., 2010).
216 SA, MSA, IA concentrations are calculated after normalizing them with the reagent ions (NO₃⁻ and
217 (HNO₃)NO₃) using the equation mentioned in Jokinen et al., 2012. The uncertainty range of the
218 measured concentrations reported in this study was estimated to be -50%/+100% and the limit of
219 detection (LOD) was 4×10^4 molecules cm⁻³ (Jokinen et al., 2012). HOMs and IA have been estimated
220 to be charged similarly at a similar kinetic limit as SA (Ehn et al., 2014; Sipilä et al., 2016), so the
221 calibration factor for them should be similar, but please note, that the concentration of other
222 compounds than SA can be highly uncertain due to different ionizing efficiencies, sensitivities and
223 other unknown uncertainties. If MSA, IA or HOMs do not ionize at the kinetic limit, these
224 concentrations could be underestimated and thus, the concentrations reported in here should be taken
225 as low limit values. The normalized signals of specific HOMs found in the study are calculated using
226 high resolution peak fitting data. Please note that the concentration of highly oxygenated molecules
227 (sum of all HOMs, monomers and dimers) were calculated from the unit mass resolution data.

228 Neutral cluster and Air Ion spectrometer (NAIS, Airel Ltd., Estonia, Manninen et al.,
229 2010; Mirme and Mirme, 2013) was used to measure the number size distribution of both positive
230 and negative ions between 0.8 nm and 42.0 nm (electric mobility diameter). The NAIS also measures
231 the number size distribution of total particles (neutral) between 2.5–42.0 nm. NAIS consists of two
232 multichannel electrical mobility analyzer columns (DMAs) operating in parallel. The columns differ
233 by the polarity of the ions measured, but are otherwise identical (Mirme and Mirme, 2013) in
234 operation. However they may differ in the transfer functions after calibration. The calibration
235 procedure for the DMAs is presented in Mirme and Mirme, 2013. The ion mode measurements are
236 corrected as in Wagner et al., 2016). The flow rate of the instrument is 60 Lpm which is split into 30
237 Lpm for each DMA. The instrument was installed in the SMEAR III station. The data was recorded
238 every 2 seconds.

239 Larger particles of 3–820 nm were measured using a twin differential mobility particle
240 sizer (DMPS) (Aalto et al., 2001). The instrument was installed in the SMEAR III station. The time
241 resolution of data is 10 minutes.

242 The size distribution of 1–3 nm particles was measured by a Particle Size Magnifier
243 (PSM, Airmodus Ltd., Finland; Vanhanen et al., 2011) in series with a condensation particle counter
244 (Airmodus Ltd., Finland). The PSM was operated by scanning the flow 0.1–1.3 lpm (continuously
245 changing the saturator flow rate), which allows determining the 1–3 nm particle concentration and
246 calculation of particle size distribution. The data was recorded for each second and the duration of
247 each scan was fixed to 240 seconds. The raw data inversion was carried out through the kernel method
248 (Chan et al., 2020; Lehtipalo et al., 2014). The raw data of the PSM employed a pretreatment filter
249 that calculates the correlation between the observed particle concentration and the saturator flow rate
250 of a single scan and discards scans with significant non-correlation or negative correlation (Chan et
251 al., 2020). Details about the Back-trajectory calculations, Chl a data analysis, meteorological and other
252 calculations of parameters such as growth rates and formation rates are explained in the SI.

253

254 **3. Results and discussions**

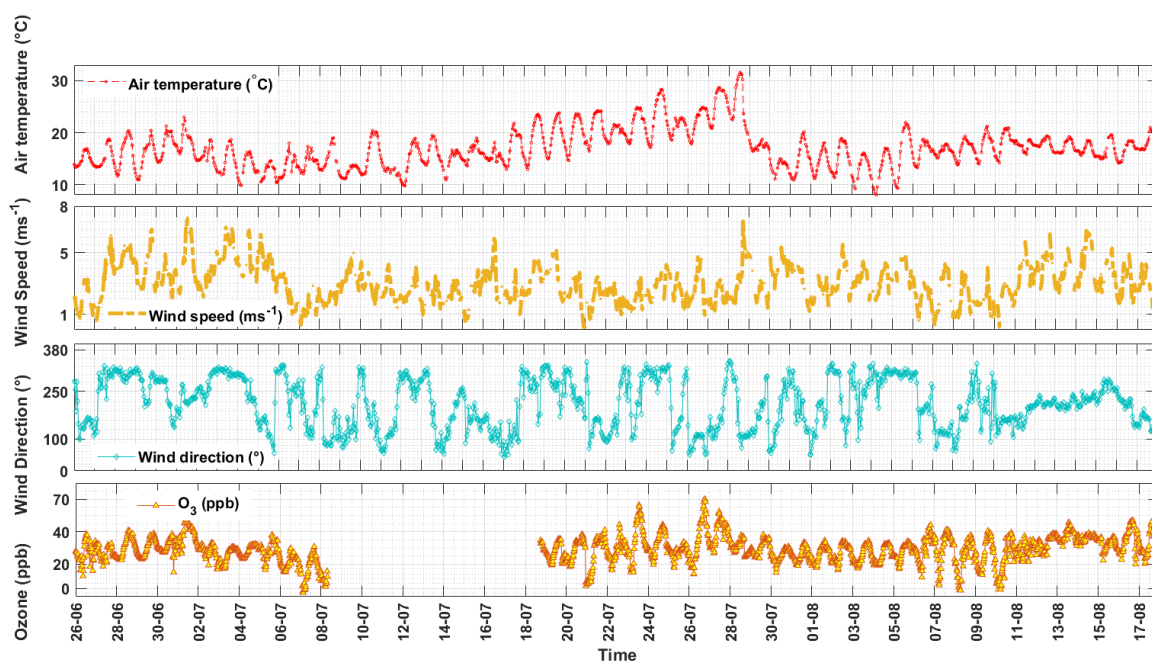
255 **3.1 Meteorological parameters and cyanobacterial bloom during the study.**

256 **3.1.1 Meteorological Parameters**

257 The meteorological parameters, especially the wind speed, wind direction and ambient temperature,
258 varied significantly during the study period. The time format in the entire study is UTC+02:00 h. This
259 study period includes the hottest summer days of Finland in year 2019. The average temperature
260 during 17–28 July 2019 (the warmest period) was 21.6° C with a maximum temperature of 31.6° C
261 recorded on the 28 July 2019 (Fig. 2). Temperature starts to decrease after 29 July 2019. The average

262 temperature in August was 16.5° C with a maximum temperature of 21.9° C recorded on 5 August
263 2019.

264 The wind direction was highly variable during June-July period. The wind direction in
265 July was mostly from the sectors 270°–320° (West-Northwest) and 90°–150° (East-South East). In
266 August, the wind gained more stability and was dominantly blowing from 180°–270° (South-West)
267 (Fig. 2). The wind speed also showed high variability in June-July. The wind speeds during June and
268 early weeks of July were mostly $>6.5 \text{ m s}^{-1}$, followed by a bit calmer mid-July (mostly $\leq 4 \text{ m s}^{-1}$)
269 with preceding high winds in end of July until mid-August (gusts of winds $> 5.2 \text{ m s}^{-1}$) (Fig. 2).
270 However, the average wind speeds in both the months was 3 m s^{-1} . The average daylight hours in July
271 were 17-18 hours with the daytime hours between 04:00–22:00 h which starts to decrease in August
272 to 15–16 hours of daylight per day (05:00 h – 21:00 h) as per the Global radiation data obtained from
273 SMEAR III station for the study period. Therefore, the actual nighttime hours in our measurement
274 site can be considered from 23:00 h–03:00 h during Finnish summers.



275
276 **Figure 2:** Time series of meteorological parameters and O₃ concentration (data from SMEAR III
277 station, 30-minute averaged) during the study period.

278 279 3.1.2 Cyanobacterial bloom conditions during the study

280 The Baltic Sea (defined from 53° N to 66° N latitude and from 10° E to 30° E longitude inclusive of
281 Gulf of Bothnia, Gulf of Finland and Gulf of Riga) is characterized by usually two algal blooms, one
282 occurring in early Spring (mostly diatoms) and then a summer bloom increasingly dominated by
283 cyanobacteria (blue green algae). The summer bloom period selected for this study was typically

284 characterized by cyanobacteria. When these microscopic cyanobacteria multiply and aggregate, they
285 are seen as blue-green patches or scum-like layers over the surface of lakes and marine waters. The
286 warm early summer temperatures (during June) resulted in a cyanobacterial bloom (Finnish national
287 monitoring; SYKE press release, 2019). However, the weather conditions in end of July began
288 changing with high winds causing the cyanobacteria to be highly mixed in the water column, which
289 reduced bloom intensity at the sea surface to lower than normal mean cyanobacterial biomass (mean
290 biomass of cyanobacteria, $105 \mu\text{g L}^{-1}$, Kownacka et al., 2020) in end of July and August (SYKE press
291 release, 2019). However the average biomass of cyanobacteria in 2019 ($196 \mu\text{g L}^{-1}$, Kownacka et al.,
292 2020) was slightly higher than the average. Subsequently, temperatures were lower in August as
293 compared to June and July and windier as compared to other summer months. These windy conditions
294 kept the lake cyanobacteria well mixed in the water. The northern Baltic Sea, including the Gulf of
295 Finland, the Southern parts of the Åland islands and even the Bothnian Sea occasionally observed
296 massive blooms of cyanobacteria during June-August 2019. However, the bloom intensity of
297 cyanobacteria at the coastal areas were intermittent and changed rapidly due to the spatial complexity
298 of the coastline and variable winds and currents.

299 These cyanobacterial blooms are generally dominated by three taxa, *Nodularia*
300 *spumigena*, *Aphanizomenon* sp. and *Dolichospermum* sp. (Knutson et al., 2016; Kownacka et al.,
301 2020). In the Baltic Sea, these cyanobacteria actually contribute the most to the total pelagic nitrogen
302 fixation (Klawonn et al., 2016). Other potential primary producers emitting vapors are the littoral
303 macroalgae growing along the shallow coastline. For example, the perennial macroalgae, *Fucus*
304 *vesiculosus* cover large areas of the coastal areas of Baltic Sea, where they support very high biomass
305 and high productivity (Attard et al., 2019). Low sea levels (0.2–0.8 m, wave height at Suomenlinna
306 aaltopoiju station, <https://en.ilmatieteenlaitos.fi/wave-height>) were recorded in mid-July (11 July
307 2019–27 July 2019) during the period when high temperatures (20°C and above) prevailed (Fig.2)
308 in our study region. During these conditions, contributors to emissions might be a mix of both coastal
309 macroalgae and open sea microalgae, which are mostly the cyanobacteria. There is a possibility that
310 reasonably large extents of coastal macroalgae, including *F. vesiculosus*, were exposed to direct
311 sunlight (in shallow waters or low tide conditions) during the decay of the blooms during mid-August
312 (when the bloom intensity was low, SYKE press release, 2019), hence making this time window
313 favorable for observing potentially high emissions in gas phase from the macroalgae, in addition to
314 the emissions from cyanobacterial blooms. However, in the semi-urban/coastal setting of this
315 measurement site, there could be various other parameters, which could also play a role in
316 determining the concentrations of the biogenic emissions; for example the wind speed and wind
317 direction. The atmosphere in this semi-urban coastal location is itself a cocktail of various vapors,

318 oxidants and particles, which would affect the quantification, source apportionment and
319 characterization of the biogenic emissions.

320

321 **3.2 Precursor vapor concentrations and their sources**

322 The measured daytime precursor vapor concentrations showed a regular diurnal cycle consistent with
323 the photochemical production of SA and IA in 90% of the days in this study. SA, key precursor of
324 atmospheric NPF, is formed mainly by reaction of sulphur dioxide with OH-radicals, which is
325 predominantly controlled by the photochemical cycles (Sipilä et al., 2010; Jokinen et al., 2017). The
326 daily mean concentration of SA in July and August were almost similar, $\sim 3 \times 10^6$ molec. cm^{-3} . The
327 mean concentration is slightly lower as compared to the concentrations of SA measured in Helsinki
328 street canyon, 1×10^7 molec. cm^{-3} (Olin et al., 2020) but similar to the SA concentration measured at
329 the SMEAR III station in 2018 (Okuljar et al., 2021). In the study of Olin et al., 2020, SA
330 concentrations were greatly affected by vehicular traffic as the site is situated at a busy street canyon.
331 The SMEAR III is considered as a background site much less affected by vehicular traffic (Okuljar
332 et al., 2021). In comparison to other locations, the daytime SA concentration in pristine Antarctic
333 region has been reported from 10^5 up to 10^7 molec. cm^{-3} (Mauldin et al., 2001, Jokinen et al., 2018),
334 10^6 molec. cm^{-3} in remote continental, remote marine and forest regions and 10^7 molec. cm^{-3} in urban
335 and rural agricultural lands using the same technique as in here (Berresheim et al., 2000; Kuang et
336 al., 2008; Petäjä et al., 2009; Kurtén et al., 2011; Zheng et al., 2011; Chen et al., 2012; Jokinen et al.,
337 2012; 2017, Kürten et al., 2014; Bianchi et al., 2016; Baalbaki et al., 2021; Dada et al., 2020). It has
338 been well documented that SA contributes to aerosol formation and growth processes (Boy et al.,
339 2008; Eisele et al., 2006; Fiedler et al., 2005; Iida et al., 2008; Sarnela et al., 2015; Jokinen et al.,
340 2018; Kürten et al., 2015, 2016; Mauldin et al., 2001; Paasonen et al., 2010; Wang et al., 2011; Weber
341 et al., 1998, 1999; Yao et al., 2018; Dada et al., 2020). Most of these studies are conclusive that SA
342 concentration in the atmosphere depends on the anthropogenic and biogenic activities around the site.

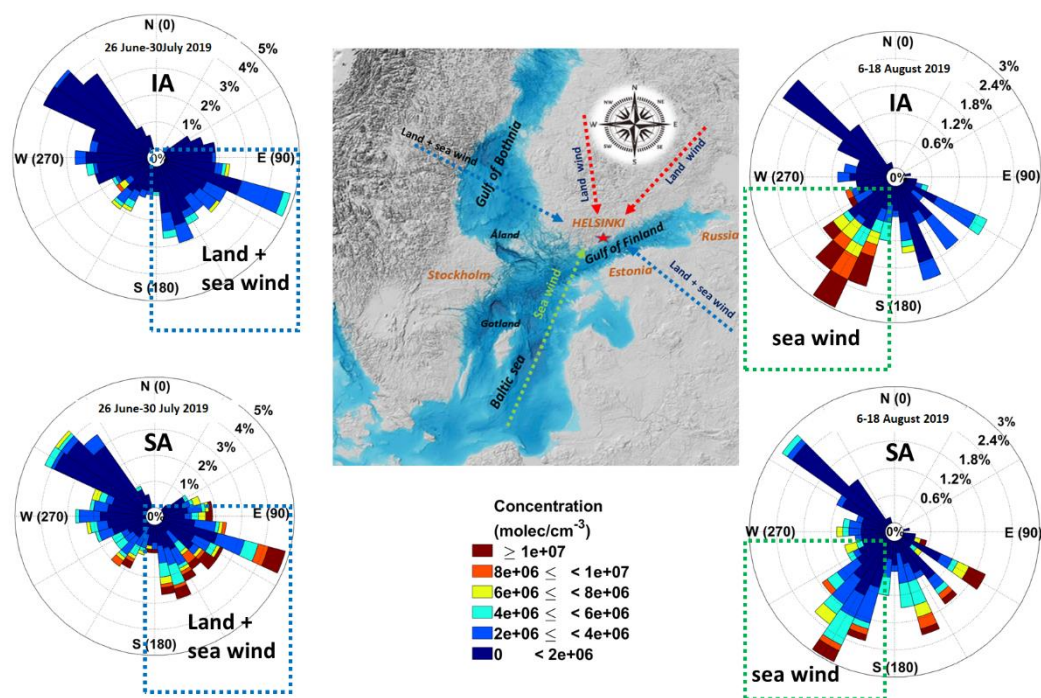
343 In the coastal marine boundary layer, the MSA concentration is typically 10–100% of
344 that of SA (Berresheim et al., 2002; Eisele and Tanner, 1993). Until recently, no studies have been
345 found to report MSA and IA concentrations in coastal/urban setting of Finland. The daily mean
346 concentration of MSA in July and August was almost similar, 4×10^5 molec. cm^{-3} . The mean
347 concentration of IA in July and August was 1×10^6 molec. cm^{-3} and 3×10^6 molec. cm^{-3} , respectively,
348 showing two times increase in IA concentrations in August (Fig. S1). A similar increase in IA
349 concentrations from summer to autumn were observed in the Arctic Ocean, where the increase in IA
350 was attributed to the freezing onset of the pack ice and increase in ozone concentrations (Baccarini et
351 al., 2020). However, here the increase is mainly due to the change in the air mass arriving at the

352 experimental site, enriched with biogenic emissions from the blooms. For the same period, the CI-
353 APiTOF data shows exceptionally high concentrations of highly oxygenated organic molecules
354 (HOMs), with monomer concentrations (300–450 amu) of 10^8 molec.cm⁻³ and HOM dimer
355 concentrations (450–600 amu) of 10^8 molec.cm⁻³ as well (Fig.S2).

356 The IA concentration rises one order of magnitude, from 10^6 to 10^7 during the 11–17
357 August 2019, when the wind direction changes abruptly (from 280°–360° to 180°–230°, marine air
358 mass, Fig. 3). We found that during the marine air (180°–230°, South Easterly, over Gulf of Finland
359 and South westerly, over Northern Baltic sea) influence over the study region, the average noontime
360 maximum of SA, IA is of the order of 10^7 molec.cm⁻³ and MSA is around 10^6 molec.cm⁻³ (Fig. 3).
361 This is one order of magnitude higher concentration than when the wind was from over the land (Fig.
362 3).

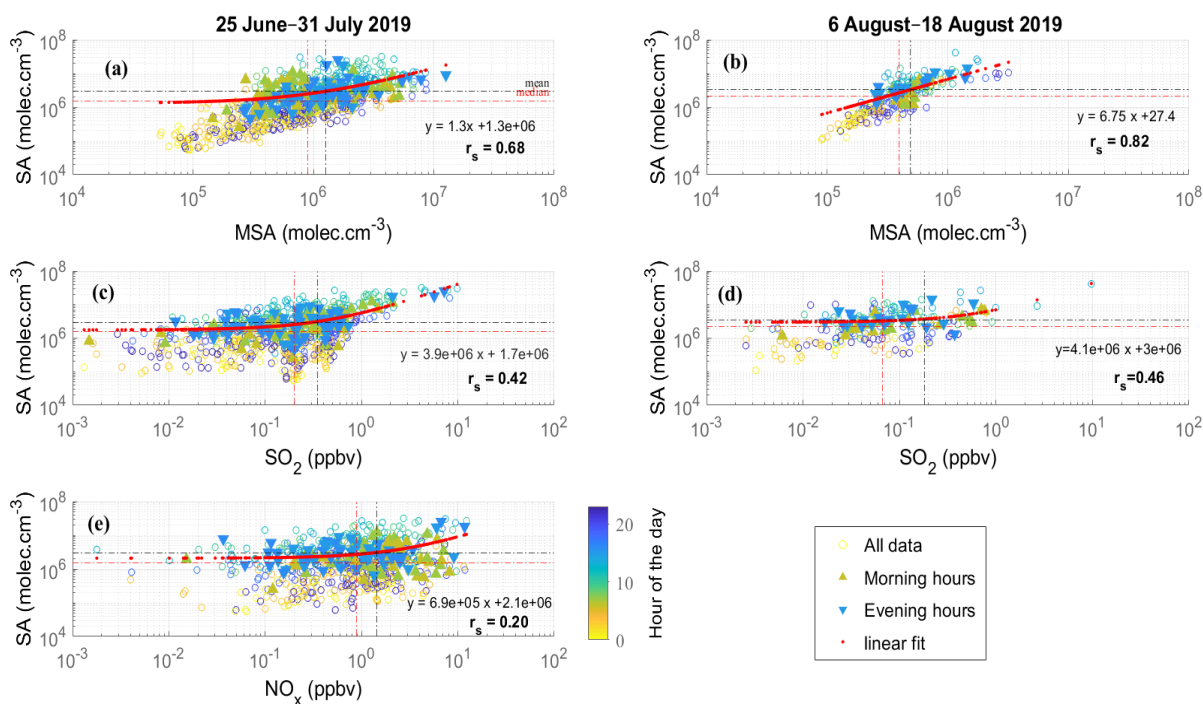
363 The highest concentration, 3×10^7 molec. cm⁻³, of IA was observed when the wind is
364 coming from the Baltic Sea sector, whereas the highest SA concentrations ($\sim 3 \times 10^7$ molec. cm⁻³) was
365 observed when air mass travelled over the countries of Estonia and Russia crossing Gulf of Finland
366 before entering the measurement site (land+sea region). The connection between the aerosol
367 precursors and the wind direction can be observed in the cases where the wind direction changes
368 rapidly. This highest IA concentration was recorded when the wind direction changes after 4 August,
369 180°–230° (the Baltic Sea region). The change in wind direction was clearly reflected in a reversal of
370 the concentration trends of SA and IA (Fig. 3). It was observed that the winds coming from 80°–180°
371 or 250°–280° (land-sea region, Fig. 3) were SA rich air masses. This comprises of the landmasses of
372 south and northeastern Finland, Northern Russia, part of Gulf of Finland and Estonia and North-North
373 western part of Finland including a part of northernmost Gulf of Bothnia. The sector 0°–90° or 280°–
374 360° (land, Fig. 3) consists mostly of urban cities.

375



376
 377 **Figure 3:** Windroses showing the variability in the concentration of gases with wind direction during
 378 the study period. Percentages on the concentric circles denote the frequency of winds from different
 379 directions. The spokes are color coded as per the concentration of the gas from the particular direction.
 380 The numbers in the parenthesis within the windroses refer to the wind direction in degrees.

381
 382 During the entire study period, when the air plume passed over the northern Baltic Sea region and the
 383 wind speed was high enough ($> 4\text{ m s}^{-1}$) high concentrations of IA was observed. While IA can be
 384 exclusively sourced from the marine and biogenic emissions (Mahajan et al., 2011; O'Dowd et al.,
 385 2002; Sipilä et al., 2016; Carpenter et al., 2021), SA could be biogenic or /and anthropogenic. Further,
 386 the temperatures prevailing during this period may have facilitated the DMS oxidation at a higher
 387 rate, which forms the source of biogenic SA and MSA. However, this is not a very simple equation,
 388 since this fractional yield of biogenic SA from DMS oxidation additionally also depends on the
 389 atmospheric NO_x ($\text{NO} + \text{NO}_2$) and HO_x ($\text{OH} + \text{HO}_2$) levels and on the scavenging of SO_2 by sea salt
 390 or cloud droplets (Hoffmann et al., 2016). The anthropogenic sources of SA for this site could also
 391 include vehicular or ship traffic especially considering that there is a city road just 250 m and a harbor
 392 6 km away from the measurement site. We explored the correlations of SA to a biogenic proxy, MSA
 393 and correlation with NO_x (anthropogenic proxy) to have a clear source apportionment of SA (Fig.4).
 394 SO_2 could not be treated entirely as anthropogenic proxy as it can be sourced from DMS oxidation as
 395 well.



396

397 **Figure 4:** Correlation of SA with MSA (a,b), SO₂ (c,d) and NO_x (e) for June–July. The black dashed
 398 lines for both axis represent the mean of the gas concentration, red dashed line represent the median
 399 value the gas concentrations and red solid line represents the linear fit. Spearman's coefficient (r_s)
 400 was used to test the correlation, at significance level, 0.001. The circles represent data points at
 401 different hours of the day. The upward pointing green triangles represent the morning rush hours
 402 (6:00–8:00 h) and the downward pointing blue triangles represent the evening rush hours (15:00–
 403 17:00 h). The yellow hollow circles represent all data. NO_x data unavailable for August.

404

405 The good correlations (r_s > 0.6, Fig. 4a and 4b) between SA and MSA during the study period
 406 (June–August) could suggest that they were sourced from a common biogenic source, the DMS
 407 emission from the cyanobacterial bloom. Good correlations of SA and MSA was also found in August
 408 (r_s = 0.8, Fig. 4b) when the air mass was mostly marine (and/or from the Finnish coastline, Fig. 3).
 409 Another observation was that SO₂ also shows some correlations with SA in both June–July and August
 410 study periods (r_s = 0.4, Fig. 4c and 4d), but not as significant as SA and MSA correlations. SO₂ can
 411 have different sources unlike MSA which is mostly biogenic. However some emissions could be
 412 sourced from agriculture and other terrestrial sources (Bates et al., 1992), hence these observations
 413 could possibly indicate SA was more from biogenic sources than from other sources. But we cannot
 414 be very accurate in this estimation only by analyzing the correlation coefficients since both MSA and
 415 SA can have a similar daily cycles due to the oxidation pathways.

416 Both SO₂ and MSA are the oxidation products of DMS (produced by phytoplanktons, including
417 some cyanobacteria), oxidized through OH and NO₃ radical (Chen et al., 2000). Some of the previous
418 chamber studies have confirmed that SO₂ is the major intermediate products formed from DMS
419 oxidation (Sørensen et al., 1996; Berresheim et al., 1995). The SO₂ could be oxidized to SA (OH/O₂
420 oxidation) during the transport. Since our experimental site was surrounded by water bodies and the
421 summer season had enriched most of these freshwater and marine waters with abundant
422 cyanobacterial blooms, this biogenic SA contribution to the study site has to be accounted when
423 analyzing the sources of SA. However, SO₂ can also be sourced from various anthropogenic activities
424 and can be oxidized to SA. In Finland the major sources of anthropogenic SO₂ is the public power
425 industries contributing to almost 90% to the total SO₂ emissions in Finland in the year 2019, while
426 transport contributing to less than 1% according to the emission inventory prepared by Finnish
427 Environment Institute, SYKE (Finnish Air Pollution Inventory; [ymparisto.fi/en-](http://ymparisto.fi/en-US/Maps_and_statistics/Air_pollutant_emissions)
428 [US/Maps_and_statistics/Air_pollutant_emissions](http://ymparisto.fi/en-US/Maps_and_statistics/Air_pollutant_emissions)). Further the maximum data points of high
429 concentrations of SO₂ ($\sim 10^7$ molec. cm⁻³) were not observed during the traffic hours in June-July-
430 August (Fig. 4c and 4d), another possible indication that biogenic sources could be contributing to
431 the SO₂ concentrations and thus SA concentrations near the study site.

432 The emission inventory of Finland for the year 2019 indicated that sources of NO_x as NO₂ were
433 mainly the power industries (41.5%) and the transport sources (41%) ([ymparisto.fi/en-](http://ymparisto.fi/en-US/Maps_and_statistics/Air_pollutant_emissions)
434 [US/Maps_and_statistics/Air_pollutant_emissions](http://ymparisto.fi/en-US/Maps_and_statistics/Air_pollutant_emissions)). These sources are indeed the most significant
435 sources of NO_x globally (Meixner and Yang, 2006). NO_x, a definitive proxy of anthropogenic
436 influence shows a poor correlation with SA ($r_s=0.28$, Fig. 4e) during June-July which could suggest
437 insignificant effect of traffic on the SA concentrations. Unfortunately, the NO_x data from August was
438 unavailable due to instrument malfunction so we cannot provide any correlations for this month.

439 The data presented in Figure 3, where we observe high SA concentrations even when the air mass
440 was marine and the good correlations of SA-MSA (inclusive of insignificant correlations of SA-NO_x)
441 (Fig. 4) indicate towards a greater possibility of the influence of biogenic emissions on the
442 concentrations of SA as compared to the anthropogenic emissions.

443

444 **3.3 Types of nucleation events during the study**

445 During 25 June 2019–19 August 2019, we observe a number of NPF events characterized by a short
446 appearance of ultrafine particles in the number size distribution lasting for less than one hour. These
447 so-called bursts /spikes appearing at small sizes (sub-3 nm) are indicative of local clustering processes
448 in contrast to regional events, where it is possible to follow the growing particle mode for several

449 hours (Dada et al., 2018; Dal Maso et al., 2005). Local clustering here means that the molecules could
 450 be transported from elsewhere but the actual clustering could have taken place near the experimental
 451 site, indicated by a small bump of clusters (with absolutely little or no growth) as seen in the NAIS
 452 spectra. We do observe transported events (events with a growing particle mode, but no small
 453 particles forming at the site) and non-events days but they are not included in the analysis. This section
 454 discusses the occurrence of local and regional new particle formation events with the focus on: 1)
 455 trace gases variability during the event days, 2) the evolution of different sized particles during these
 456 events, 3) the impact of meteorological parameters and 4) the effect of cyanobacterial bloom on the
 457 events.

458

459 **Table 1:** Timing and maximum concentration of SA, MSA and IA during local and burst/spike

460

nucleation events during the study period

Dates	Type of Event	time of NPF (UTC+02:00 h)	SA (max) molec. cm ⁻³	MSA (max) molec. cm ⁻³	IA(max) molec. cm ⁻³
30 June 2019	Regional/local	8:45–13:23 14:00–16:30	7.9×10 ⁶	5.6×10 ⁵	2.3×10 ⁶
30 July 2019	Regional/local	7:45–11:16	1.2×10 ⁷	1.2×10 ⁶	5.3×10 ⁶
11 August 2019	Ion Burst (Spike)	13:40–14:32	1.0×10 ⁷	1×10 ⁶	3.2×10 ⁷
14 August 2019	Ion Burst (Spikes)	8:00–8:20	4.2×10 ⁶	5.3×10 ⁵	8.5×10 ⁶
15 August 2019	Multiple Ion Bursts (Spikes)	6:00, 8:58, 14:00–16:00	6.4×10 ⁶ 6.3×10 ⁶ 7.0×10 ⁶	5.8×10 ⁵ 4.6×10 ⁵ 6.8×10 ⁵	2.5×10 ⁶ 3.1×10 ⁶ 1.5×10 ⁶

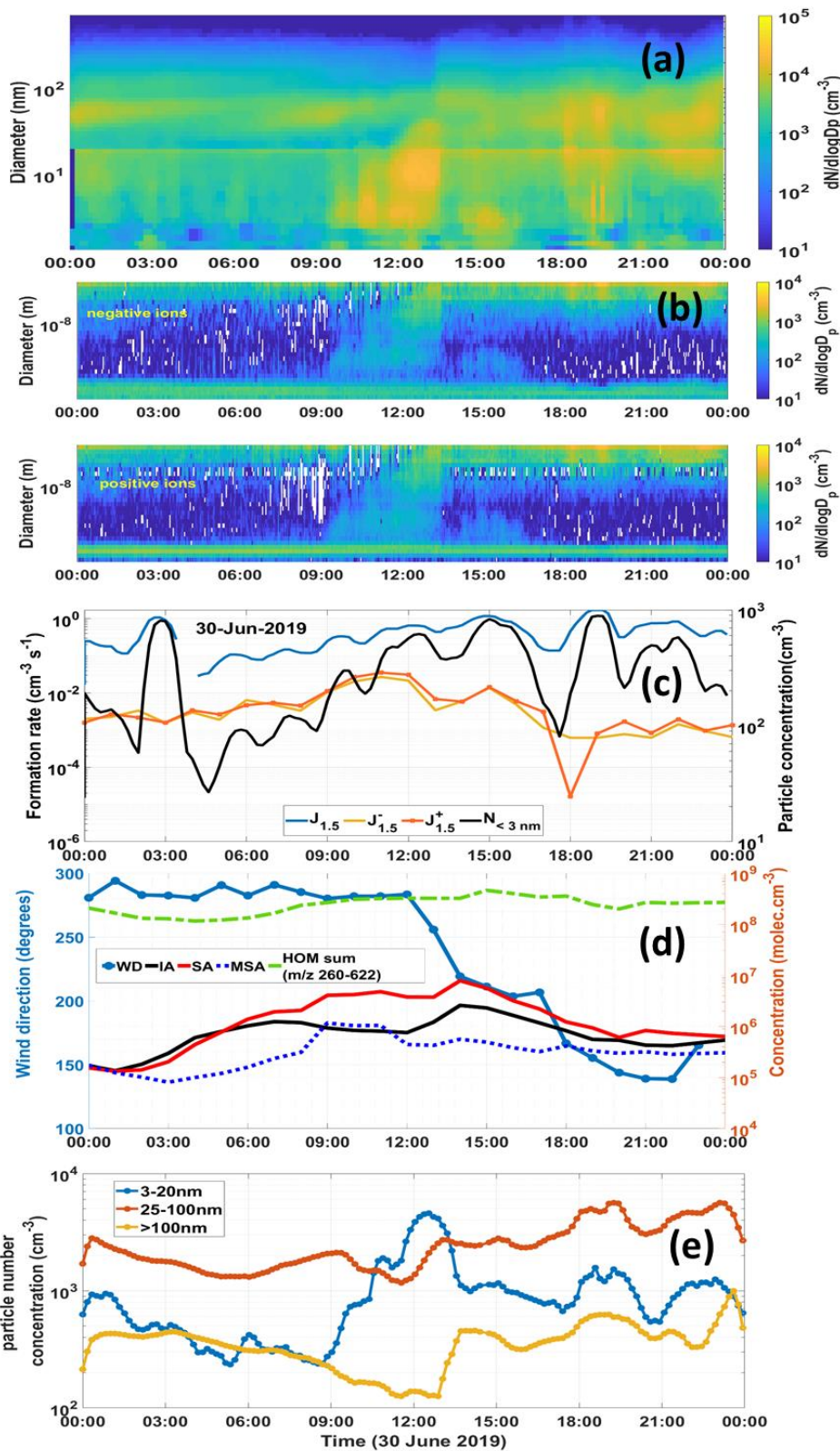
461

462 3.3.1 Nucleation: Regional and Local events

463 A regional NPF event was observed on 30 June 2019, which starts at 08:45 h and ends at 13:23 h (Fig
 464 5a). The negative ion clusters start to increase in concentration first at 08:45 h (Fig. 5b) concurrent
 465 with the increase in concentration of the smallest particles (<3nm) from 10² to 10³ cm⁻³ (Fig. 5c).
 466 Preceding the NPF event the SA concentrations were steadily increasing and subsequently at 09:00
 467 h, SA concentration doubles from 2×10⁶ to 4×10⁶ molec. cm⁻³ (Fig. 5d), while the particle formation

468 rate at 1.5 nm ($J_{1.5}$) increased from $0.3 \text{ cm}^{-3} \text{ s}^{-1}$ to $0.6 \text{ cm}^{-3} \text{ s}^{-1}$. $J_{1.5}$ was much higher than either of
469 $J_{+1.5}$ and $J_{-1.5}$, thus indicating a neutral formation pathway rather than ion mediated. Further we also
470 observe local clustering event at 15:00 h with simultaneous increase of concentration of SA and
471 HOMs along with increase in the smallest particle concentration. This possibly indicates the role of
472 SA and HOMs in the nucleation initiation. The high normalized signals of DMA-SA cluster seen
473 during the entire event (increasing from the start of NPF event) possibly indicates that SA clusters
474 initiate the event (Fig. S4a). DMA inclusive of other main methylamines like mono and tri
475 methylamines (Bergman et al., 2015) in the global inventory (Schade and Crutzen, 1995) is
476 contributed through the animal husbandry and other agricultural practices, biomass burning and some
477 contributions from marine and terrestrial sources. Although among these methylamine emissions,
478 generally the trimethylamine dominates (Schade and Crutzen, 1995). Although no estimates of DMA
479 measurements are available from Helsinki region, the DMA in a boreal forest site in Finland has been
480 estimated to be below $\sim 150 \text{ ppqV}$ (Sipilä et al., 2015), measured through a NO_3^- -chemical ionization
481 mass spectrometer. Their work also stated that DMA was unlikely the playing an important role in
482 the nucleation process observed at the site.

483 The increase of HOMs is also clearly observed during the event Fig. S4b. Therefore we
484 suggest that nucleation and growth of particles was possibly due to SA-organics which ensures that
485 particles reach the CCN and thus climate relevant diameters. The work of Okuljar et al. (2021) also
486 report an increase in sub-3 nm particles with a simultaneous increase in SA concentration at the
487 SMEAR III site, supporting our observations. However, the role of HOMs in nucleation initiation has
488 not been explored at this site.

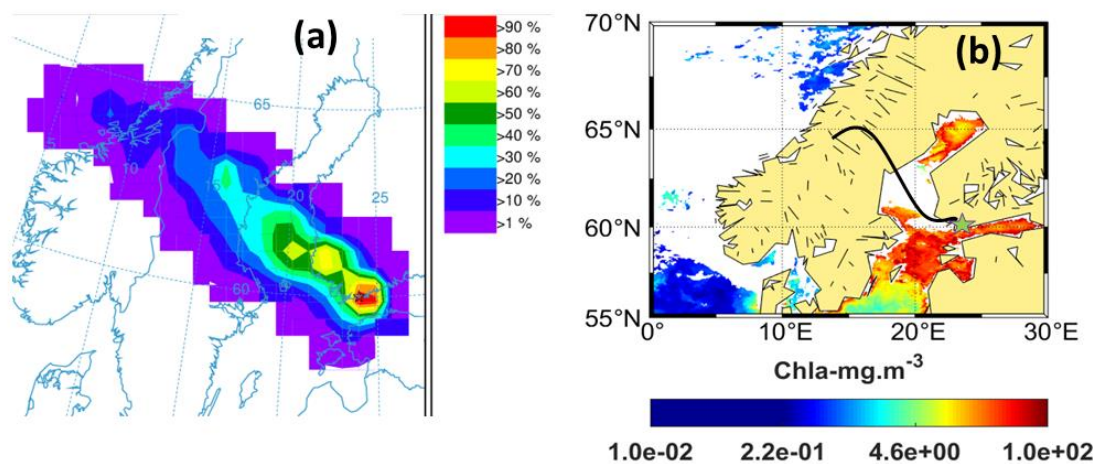


489

490

491 **Figure 5:** NPF Event (Regional and local events), 30 June 2019. (a) Number size distribution of
 492 particles (data from PSM, NAIS and DMPS; size range: sub-3–100nm). (b) Charged particles number
 493 size distribution (negative: upper, positive: lower) obtained from the NAIS. (c) Diurnal variation of

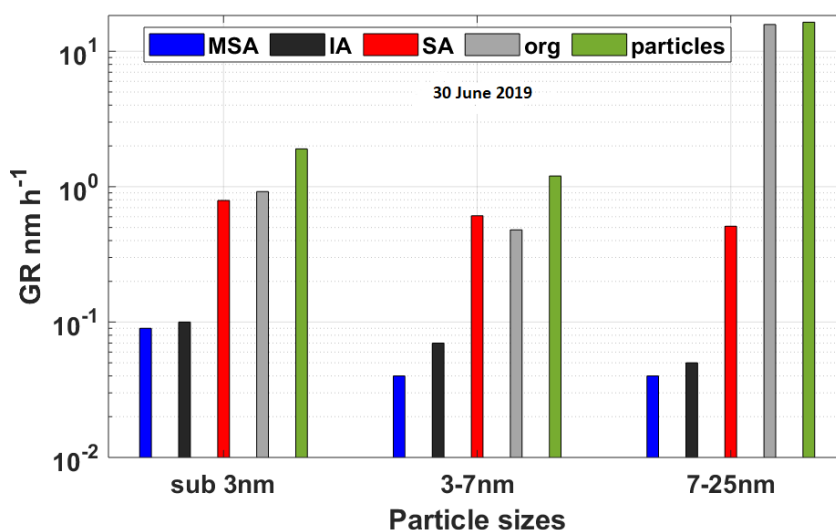
494 formation rates ($J_{1.5}$) of 1.5 nm particles and ions ($J_{1.5}$ and $J^{+}_{1.5}$) on the left axis and particle number
 495 concentrations (1.5–3 nm) on the right axis. (d) Diurnal variation of HOMs, SA, IA and MSA with
 496 wind direction (WD). (e) The diurnal variation of particle concentration in nucleation:3–20 nm;
 497 aitken: 25–100 nm and accumulation: >100nm) mode particles during the event (Data from DMPS).



498
 499
 500 **Figure 6:** (a) Trajectory frequency plot (100 a.g.l, arrival time of trajectories at the measurement site:
 501 20:00 h) for 24 h back trajectory using GDAS meteorological input data (frequency grid resolution:
 502 $1.0^{\circ} \times 1.0^{\circ}$) (b) Chl-*a* concentrations (GlobColour level-3); Black line shows the trajectory direction and the star point denotes the measurement site .

504
 505 A clear increase in nucleation mode particles is seen during the event, starting at 08:45 h (234 cm^{-3})
 506 and reaching its maximum at 12:30 h (4589 cm^{-3}). This increase in concentration of the nucleation
 507 mode particles was followed by the increase in concentration of Aitken mode and accumulation mode
 508 particles and continues for a couple of hours, indicating growth of particles (Fig. 5e), possibly
 509 reaching to CCN relevant sizes. However, we also observe a drop in Aitken particles before NPF
 510 which also continues during NPF. We speculate it could be due to the change in wind direction
 511 (Väkevä et al., 2000) before NPF. The wind direction relatively remains constant throughout the NPF
 512 so the low concentration of Aitken mode continues. Wind direction changes abruptly at 12:00 h and
 513 the Aitken mode particle concentrations increases soon after this change of wind direction (Fig. 5d).
 514 This shows the particles must be in the process of growth mostly elsewhere, which is not evident in
 515 the changed air mass, however we still observe almost the same (or even slightly higher) precursor
 516 vapor concentrations, since the wind still passed over the bloom areas before entering our study site.
 517 After the change in local wind direction, the observed SA and IA slightly increase, and we still
 518 observe clustering (formation of small ions and particles), but no continuous growth typical for

519 regional events. Figure 6a shows that >40% of the trajectories passes above the Swedish island of
 520 Gotland towards southern part of Bothnian Sea. The satellite data shows that the bloom was present
 521 in the Bothnian Sea, but not quite dense as compared to the southern Baltic Sea (south of Gotland
 522 island) and the northern part of the Gulf of Finland (Fig. 6b). The majority of the trajectories did not
 523 pass over the dense cyanobacterial bloom patch during this day (Fig. 6b). The calculated normalized
 524 residence time was higher over the neighboring cities of Helsinki (Southwestern side) and parts of
 525 Bothnian Sea during the event time (see Fig. S3). Thus the land based anthropogenic activities and
 526 biogenic sources both can be contributing to SA concentrations for this event; here we cannot exactly
 527 quantify the source types for SA. However, the source of SA from the local sources such as vehicular
 528 traffic around our measurement site is small (as discussed above) but cannot be completely ignored
 529 (Olin et al., 2020).



530
 531 **Figure 7:** Particle growth rates calculated from the kinetic condensation of gases (data from CI-APi-
 532 ToF) and the measured particle GRs (data from NAIS) in different size classes on 30 June 2019.

533
 534 The particle GR (7–25 nm) for this event was 16.5 nm h⁻¹, which is typical of a coastal
 535 site. Even when several condensing vapors participate in the growth process, growth rates typically
 536 do not exceed 20 nm h⁻¹ (Kulmala et al., 2004). The GR for organics was calculated after subtracting
 537 the combined contribution of the GR of SA, IA and MSA from the measured particle GR (Fig. 7).
 538 The GR for organics should be treated as an estimation since no separate GR calculations and
 539 assumptions were used. The calculated growth rates (GR) shows that SA can explain maximum 41%
 540 of the growth of sub-3 nm particles, while IA and MSA can explain only <1% of the GR in this size
 541 range. The GR by SA in the bigger size fraction (7–25 nm) was only 0.51 nm h⁻¹ explaining only 3%
 542 of the measured growth rate of particles. This means that vapors other than SA, IA and MSA were

543 responsible for 96% of the measured particle growth. These other vapors could include different
544 organics, since they are known to contribute to growth of particles (Kulmala et al., 1998, 2004;
545 Riipinen et al., 2012; Zheng et al., 2020) and could better explain particle growth in the boreal forest
546 (Ehn et al., 2014).

547 Another example of regional event (neutral nucleation) probably driven by SA and organics was
548 observed on 30 July 2019 (Fig. S5) which lasts for around four hours. The trajectory frequency plots
549 showed that most of the trajectories were from the northern land areas (including urban cities and
550 boreal forests) of Finland with highest residence times over these land regions (Fig. S6 and S7). Since,
551 the precursor gases from the biogenic origin, IA and MSA, do not show a significant concentration
552 increase as compared to SA, at the start of the event, their contribution towards the initiation of the
553 NPF event may not be as significant as SA. The greater residence times over the land areas clearly
554 support the high SA and organic concentrations seen during the event indicating a SA driven event –
555 with a possible contribution of HOMs (Fig. S7). In this case, SA explains 60% of growth of sub-3nm
556 particles compared to 41% when the dominating trajectories passed over the Gulf of Finland (Fig. 5,
557 30 June 2019). Still, as for the previous case, a major fraction of the growth in the 3–7 nm range
558 remains unexplained by the available acids (SA, IA, MSA) and is expected to be related to the
559 contribution of organics. The GRs explained by SA in both sub-3 nm (1.93 nm h^{-1}) and 3–7 nm (1.46
560 nm h^{-1}) size ranges are 58-59% higher than on 30 June 2019 (0.79 nm h^{-1} and 0.61 nm h^{-1} for sub-3
561 nm and 3–7 nm, respectively) which could be explained by the increase in SA by 52% on 30 July
562 2019. Thus, the events on 30 June and 30 July possibly occur via the nucleation of SA (possibly
563 stabilized by bases eg. ammonia or amines) and the HOMs contribute to growth of particles and
564 possibly in nucleation as well.

565

566 **3.3.2 Nucleation: Burst events**

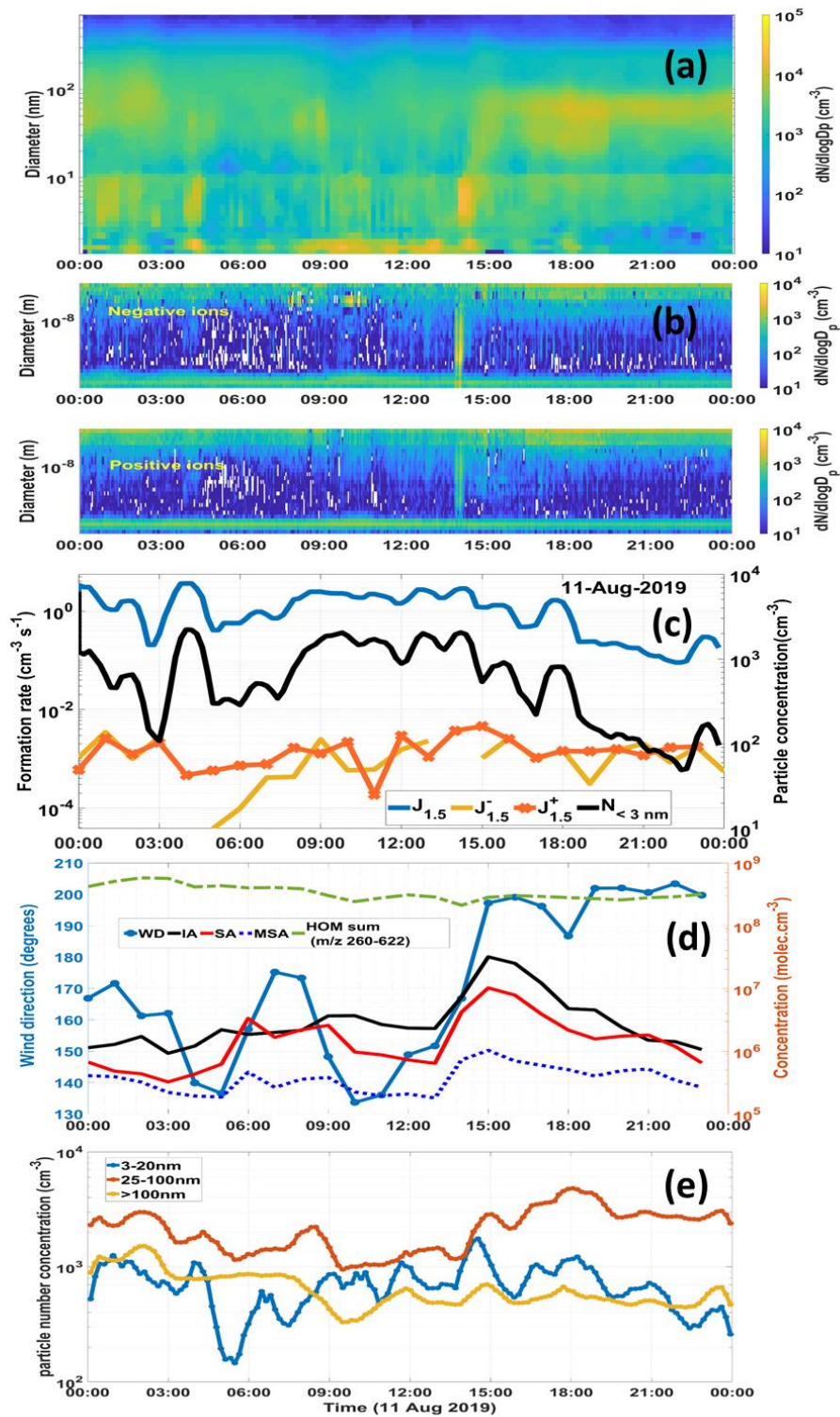
567 **Case 1: Biogenic IA nucleation- burst/spike events, 11 August.2019**

568 Intense burst events are frequently observed at coastal sites accompanied with high concentrations of
569 IA (O'Dowd et al., 2002; Rong et al., 2020; Sipilä et al., 2016). Two of such bursts or spike events
570 were observed on 11 August 2019 at 04:00 h and 13:00 h (Fig. 8a). Only the second spike event was
571 observed in the NAIS size distribution with a higher intensity in the negative ion mode at 13:00 h
572 (Fig. 8b). During both these spike events we observe the formation of clusters (1.5 nm) and the
573 formation rate ($J_{1.5}$) increases from 0.2 to $3.7 \text{ cm}^{-3}\text{s}^{-1}$ during the event with a simultaneous significant
574 increase in the sub-3 nm particle concentrations from ~ 100 to $>2000 \text{ cm}^{-3}$ (Fig. 8c). $J_{1.5}^+$ and $J_{1.5}^-$
575 remain lower than the total formation rate indicating this event to be a case of neutral nucleation. At
576 the same time, IA shows increase in concentration from $9 \times 10^5 \text{ molec. cm}^{-3}$ at 03:00 h to $1 \times 10^6 \text{ molec.}$

577 cm^{-3} at 04:00 h. During this event the air masses changes from 160° to 140° i.e the direction of the
578 air mass is changed to the Gulf of Finland. In the second burst (at 13:00 h), the IA concentration
579 increases from 2×10^6 to 7×10^6 molec. cm^{-3} from 13:00 h to 14:00 h (Fig. 8d) with a slight change in
580 wind direction from 151° to 166° . Most of these air masses are from the Gulf of Finland. SA
581 concentration also increased but remained lower than IA during both the burst/spike events indicating
582 a possibility that iodine oxoacid formation initiates cluster formation (He et al., 2021). We observe a
583 growth of particles until 15:00 h in the particle modes (NAIS data, Fig. 7b). However, the particles
584 are seen reaching sizes up to size 100 nm (DMPS data, Fig. 8a). The organics almost remain constant
585 within the range of $2\text{--}3 \times 10^8$ molec. cm^{-3} . A further increase in IA concentration, 3×10^7 molec. cm^{-3}
586 occurs at 15:00 h, and the concentration remains in the range of 10^7 molec. cm^{-3} for another two hours
587 (Fig. 8d). This was the highest observed IA concentration in the entire measurement period. A recent
588 study by He et al., 2021, indicate that IA concentrations above 1×10^7 molec. cm^{-3} leads to rapid new
589 particle formation at $+10^\circ$ C. At such concentrations the efficacy of iodine oxoacids to form new
590 particles exceeds that of the $\text{H}_2\text{SO}_4\text{--NH}_3$ system at the same acid concentrations. Thus, the
591 concentration of IA found in this event (two times higher than SA during the start of the event), the
592 high formation rates ($>1 \text{ cm}^{-3} \text{ s}^{-1}$) and an unchanged concentration of SA during the event, as
593 compared to the event on 30 June 2019, strongly suggests that it could be an IA driven-NPF event.
594 In addition, a clear increase in the normalized signal of deprotonated IO_3^- with no significant increase
595 in DMA-SA cluster is noted at 13:00 h (Fig. S8a). However, $\text{HNO}_3\text{--IO}_3^-$ cluster was the most
596 abundant followed by the $\text{H}_2\text{O--IO}_3^-$ cluster, indicating this event to be IA-driven nucleation. Further,
597 between 14:00–15:00 h, when we observe the highest IA concentrations a subsequent growth of
598 particles is noted. We also observe an increasing number concentration of nucleation mode particles
599 from 13:40 h ($\sim 650 \text{ cm}^{-3}$) to 14:40 h ($\sim 1800 \text{ cm}^{-3}$). After this one hour of intense clustering, the Aitken
600 mode particles also begin to increase in concentration from $\sim 1300 \text{ cm}^{-3}$ to $\sim 4800 \text{ cm}^{-3}$ during 15:00
601 h–18:00 h (Fig. 8e). The total particle concentration increased from $\sim 2400 \text{ cm}^{-3}$ to $\sim 6400 \text{ cm}^{-3}$ within
602 an hour during this burst event. We suggest that this burst event was possibly capable of producing
603 particles big enough to act as CCN. Since it was an intense burst event with no proper horizontal
604 growth (as seen in “banana” type events), we were not able to calculate the growth rate for this
605 particular event. Therefore we are unable to quantify the contribution of IA towards the growth of
606 particles reaching CCN sizes.

607

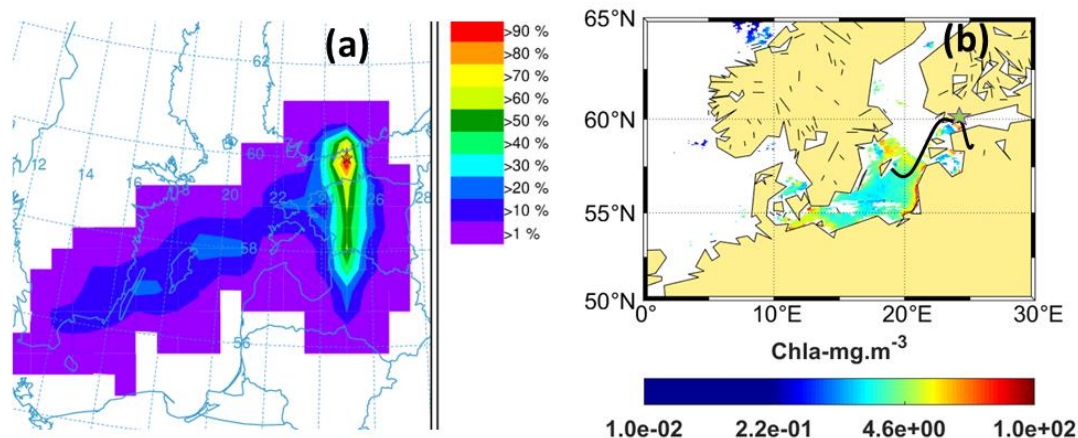
608



609

610 **Figure 8:** Burst/Event, 11 August 2019. (a) Number size distribution of particles (data from PSM,
 611 NAIS and DMPS; size range: 1–100 nm). (b) Charged particles number size distribution (negative:
 612 upper, positive: lower) obtained from the NAIS. (c) Diurnal variation of formation rates ($J_{1.5}$) of 1.5
 613 nm particles and ions ($J_{1.5}^-$ and $J_{1.5}^+$) and total number concentrations of particles (<3 nm, PSM). (d)
 614 Diurnal variation of HOMs, SA, IA and MSA with wind direction (WD). (e) The diurnal variation of

615 particle concentration in nucleation (3–20 nm), Aitken (25–100 nm) and accumulation mode (>100
616 nm) particles (DMPS data).



617

618

619 **Figure: 9** (a) Trajectory frequency plot (100 a.g.l, arrival time of trajectories at measurement site:
620 22:00 h) for 24 hour back trajectory using GDAS meteorological input data (frequency grid
621 resolution: $1.0^{\circ} \times 1.0^{\circ}$) (b) Chl-*a* concentrations (GlobColour level-3); Black line shows the trajectory
622 direction and the star point denotes the measurement site.

623

624 The global radiation and brightness parameter suggests that 11 August 2019 was overall
625 cloudy until 12:30 h (Fig. S9). The weather starts to turn into clear-sky after 13:00 h when the
626 brightness parameter increases from <0.3 to ~0.7 (Fig. S9). Impact of brightness parameter on NPF
627 was also observed in a previous study (Dada et al. 2017). The clearing of the sky could explain the
628 intense spike at 13:00 h in the particle number size distribution as well as in the acid concentrations.
629 For this particular case, we investigated further the source of such high IA concentrations and we
630 found that during this day, the maximum frequency of trajectories was observed over southern Gulf
631 of Finland (inclusive of the coastal waters of Suomenlinna island) however we do see the air masses
632 coming in from the central Baltic Sea as well which was characterized by intense bloom during this
633 day (Fig. 9a). Interestingly, the cyanobacterial bloom was observed in three intense patches in the
634 central Baltic Sea, southern Gulf of Finland (ship transect route between Helsinki and Tallinn) and
635 Gulf of Riga (Fig. 9b). The sea level was also low as it was observed to be 0.8–0.9 m in the coastal
636 waters in around the measurement site (Suomenlinna and Gulf of Finland coastal measurements
637 sites), supporting the exposure of the macroalgae to sunlight which can be a good source of iodine
638 precursors.

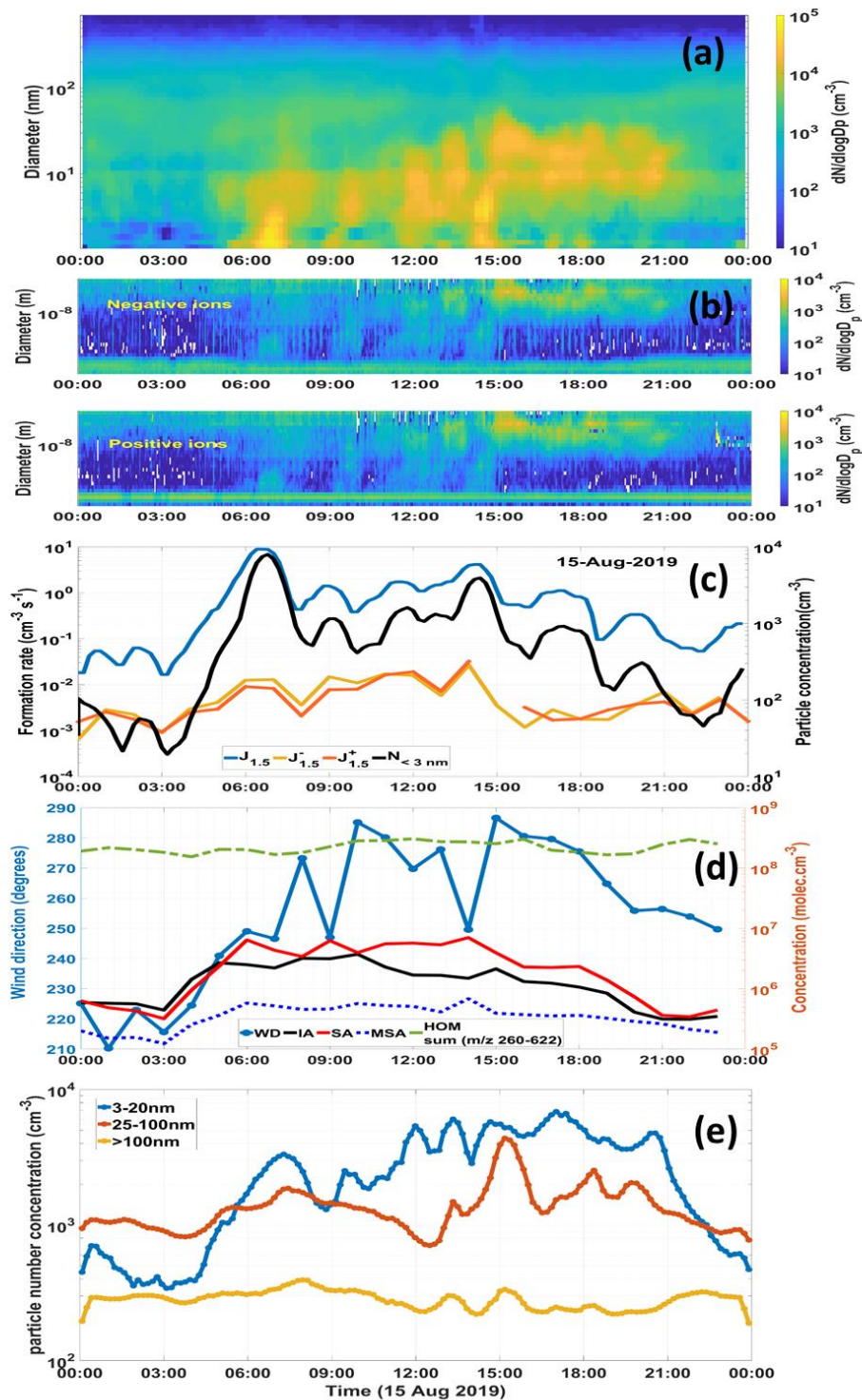
639 The residence time of the air masses coming from the Gulf of Finland and Baltic Sea
640 were longer than the residence time of the air masses coming from the neighboring land areas (Fig.
641 S10) clearly explaining the source of high IA observed during the event, which is through the blooms.
642 Further, the air mass was completely marine at 15:00 h when the highest IA is recorded supportive
643 of the marine biogenic source of IA and its transport to the measurement site. The distance from the
644 Gulf of Finland to the measurement site is approximately 5-10 km. With the wind speed of 5 m s^{-1}
645 recorded during the event, it takes less than one hour for the emission to transfer to our measurement
646 site. By the time the air mass reached our measurement site from the emission source, a fraction of
647 the emitted I_2 could have oxidized to IA. However, at this point we cannot differentiate between the
648 sources of IA from neighboring coastal waters and the central Baltic Sea but can speculate that most
649 of the IA observed could be sourced from the nearest coastal locations of Gulf of Finland.

650 Another burst/spike event driven by IA occurred on 14 August 2019 (Fig. S11) when
651 the IA concentration was found to be $8 \times 10^6 \text{ molec.cm}^{-3}$, which was 2 times higher than SA
652 concentration ($4 \times 10^6 \text{ molec.cm}^{-3}$). The event did not last more than 30 minutes. The precursor vapor
653 concentration was not large enough for the event to continue or the particles to grow further. The
654 meteorological conditions were very much similar to this event (11 August 2019). For this event also,
655 the air mass was marine with maximum residence times over the Gulf of Finland and Baltic Sea
656 regions. Vicinity of the emissions to the measurement site enabled the detection of these fast-forming
657 clusters.

658 **Case 2: Biogenic SA nucleation –multiple bursts events**

659 Another kind of event was observed on 15 August 2019 (Fig. 10a) where multiple particle bursts are
660 observed and the particles grow to sizes $> 50 \text{ nm}$.

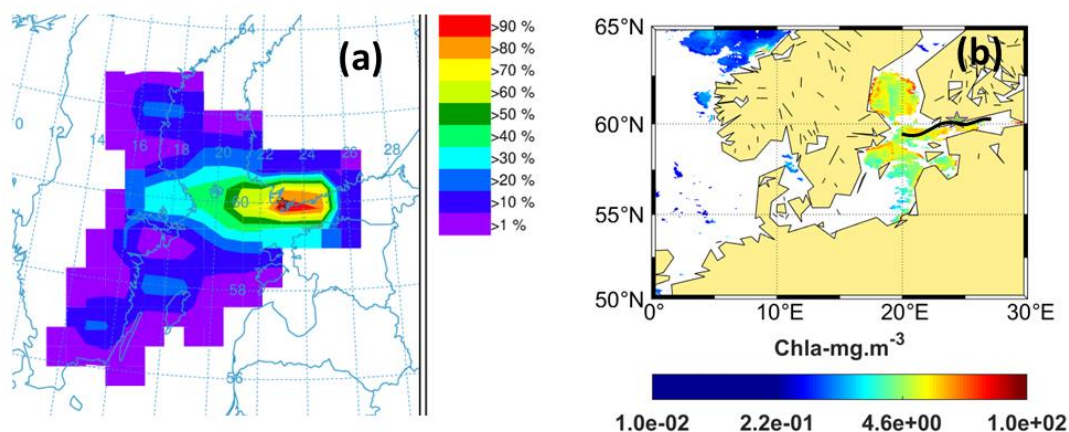
661



662

663 **Figure 10:** Multiple Burst/Spikes, 15 August 2019. (a) Number size distribution of particles (data
 664 from PSM, NAIS and DMPS; size range: 1–100nm). (b) Charged particles number size distribution
 665 (negative: upper, positive: lower) obtained from the NAIS. (c) Diurnal variation of formation rates
 666 ($J_{1.5}$) of 1.5 nm particles and ions ($J_{1.5}^-$ and $J_{1.5}^+$) and total number concentrations of particles (<3 nm,
 667 PSM). (d) Diurnal variation of HOMs SA, IA and MSA with wind direction (WD). (e) The diurnal

668 variation of particle concentration in nucleation (3–20 nm), Aitken (25–100 nm) and accumulation
669 mode (>100 nm) particles (DMPS data).



670

671

672 **Figure 11:** (a) Trajectory frequency plot (100 a.g.l, arrival time of trajectories at the measurement
673 site: 22:00 h) for 24 h back trajectory using GDAS meteorological input data (frequency grid
674 resolution: $1.0^\circ \times 1.0^\circ$) (b) Chl-*a* concentrations (GlobColour level-3); Black line shows the trajectory
675 direction and the star point denotes the measurement site.

676

677 The formation rates for the smallest clusters for both the polarities were the same ($J_{1.5^+}$ and $J_{1.5^-}$) (Fig.
678 10b and c). This was also a case of neutral nucleation as inferred from the relatively high (as compared
679 to ions) $J_{1.5}$ (neutrals). On 15 August there was a sudden change of wind direction from the 180° –
680 215° (prominent wind direction during 11–14 August 2019) to 280° and a series of bursts is triggered
681 with the intense formation of clusters (<3 nm) at each burst (Fig. 10d). The two most intense burst
682 events were associated with an increase in SA from 2 to 6×10^6 molec. cm^{-3} at 06:00 h, and 5 to 7
683 $\times 10^6$ molec. cm^{-3} at 14:00 h (Fig. 10d). A third burst at 09:00 h showed an increase in SA from 3 to
684 6×10^6 molec. cm^{-3} and interestingly the concentration of IA_{max} increased to 3×10^6 molec. cm^{-3} . In all
685 the three bursts a simultaneous increase in IA and MSA from 03:00 h to 12:00 h is observed, with the
686 SA concentration being two to three times higher than IA and four to five times higher than MSA
687 concentrations. The most intensive burst was at 14:00 h (as compared burst to 6:00 h) when the SA
688 was 3 times higher than IA. This burst was associated with a significant increase in Aitken mode
689 particle concentration (from 1490 cm^{-3} at 14:00 h to 4300 cm^{-3} at 15:00 h). The increase in
690 accumulation particle concentration was seen just after one hour from the start of the bursts for both
691 events (06:00 h and 14:00 h). However the increase in accumulation mode particle concentration for
692 these two events was not very significant ($\sim 100 \text{ cm}^{-3}$) although particles reaching a size more than 80

693 nm (CCN relevant sizes) was observed. We saw DMA-SA clusters during the event (Fig. S12) which
694 supports the observation that this a SA-driven NPF event.

695 During both these events (in fact, all the smaller burst events observed during this day), the
696 trajectories were originating from Sweden (24 h prior to arrival). However, before entering the
697 measurement site the trajectories passed over the Southern part of Gulf of Bothnia and the trajectory
698 frequency was >70% when the wind passed over the cyanobacterial bloom region (Fig. 11a and b).
699 To confirm our findings we checked a day where there was less intense bloom in the Gulf of Finland
700 and Northern Baltic Sea and the dominant air mass did not pass over the bloom patch in Gulf of
701 Finland (Fig. S13) before entering our experimental site. We did not observe an NPF event on this
702 day, thereby suggesting that the air masses passing over the bloom patches before arriving at our
703 study site were bringing in biogenic precursor vapors capable of initiating NPF events.

704

705 **3.4 Possible contributions of biogenic emissions to Precursor gaseous vapors**

706 Assuming insignificant anthropogenic SA contribution as discussed in section 3.2, we investigated
707 the other possible sources of SA by evaluating the type of algae present in the water bodies from
708 where the air masses travelled during the events. The marine algae produces
709 dimethylsulfoniopropionate (DMSP), which is capable of forming DMS, which subsequently
710 oxidizes into SA and MSA. Very few cyanobacterial species are capable of producing DMSP
711 (Karsten et al., 1996; Jonkers et al., 1998), and its concentration can vary considerably from one
712 species to another (Keller et al., 1989). Moreover, blooms could be well-mixed with other algal
713 species (ESA report, 2000) which are capable of producing DMSP. A recent experiment identified
714 *Aphanizomenon* as the only cyanobacteria producing DMS (Steinke et al., 2018). The Gulfs of
715 Bothnia and Riga are dominated by the genus *Aphanizomenon* (Kownacka et al., 2020). In addition,
716 the Bothnian Sea and Gulf of Finland were found to be rich in cyanobacterial genera of
717 *Aphanizomenon* along with *Nodularia* and *Dolichospermum* (Kownacka et al., 2020). As per the
718 previous studies which were carried out as part of the Baltic-wide monitoring (Kowancka et al., 2020
719 and the references mentioned therein), bloom composition is fairly consistent for different regions
720 and seasons from year to year, which makes it possible for us to make close estimations of the species
721 present during our study in a particular region (from where the air mass travels and the residence time
722 over a particular region).

723 A recent study also indicated that the abundance of DMS producing cyanobacteria,
724 *Aphanizomenon* has increased in the Bothnian Sea due to decreasing salinity (Olofsson et al., 2020).
725 Moreover, marine waters themselves are a large source of DMS (Kettle and Andreae, 2000)

726 explaining the contribution of biogenic SA in the above-mentioned burst events (15 August 2019).
727 Hence to conclude, the marine regions surrounding the experimental site could be potential sources
728 of biogenic SA. Moreover, high iodine emissions could be expected over the Baltic Sea region due
729 to the presence of the macroalgal species which are well established and adapted there despite its low
730 salinity (Kautsky and Kautsky, 2000; Schagerström et al., 2014) (Note the high IA on 11 August
731 2019, event day). The rocky shorelines of the northern Baltic Sea provides ample habitat for several
732 species of macroalgae, including *F. vesiculosus* (Kautsky & Kautsky 2000, Torn et al., 2006).
733 Previous studies have documented that certain macroalgae contain high levels of iodine (Ar Gall et
734 al., 2004), of which the kelp *Laminaria digitata* stores the highest amount (Ar Gall et al., 2004;
735 Küpper et al., 1998). A recent chamber experiment comparing different species of brown algae found
736 that emission rate of I₂ was higher in the case of *F. vesiculosus* when compared to other species like
737 *L. digitata* (Huang et al., 2013). This could possibly explain the high IA concentration recorded by
738 the CI-APiTOF when the air mass was coming from the Northern Baltic Sea (11 August 2019 and 14
739 August 2019). High production of macroalgal species is common along the extensive archipelago
740 coastlines of the northern Baltic Sea, and particularly *F. vesiculosus* is likely to contribute with high
741 emission rates, especially during peak production times when exposed to low sea-levels and direct
742 sunlight. However, partitioning the influence of macroalgae and microalage requires further
743 mechanistic studies. We suggest that marine and coastal regions surrounding the measurement site
744 are capable of producing SA and IA during bloom period, which can initiate NPF.

745

746 **4 Conclusions**

747 We studied the composition, concentrations and sources of precursor vapors forming aerosols in
748 Helsinki, Finland during the summer of 2019. The source of precursor gases responsible for new
749 particle formations were assessed by analyzing the meteorological parameters and situation of
750 cyanobacterial/algal bloom in the Baltic Sea. Our study recorded several regional, local and burst
751 events and we found that they were connected to elevated concentrations of SA and IA. The burst
752 /spike events occurred simultaneously with high intensity cyanobacterial/algal blooms in the Baltic
753 Sea.

754 The study draws the following conclusions. 1) Constantly changing algal conditions in
755 Gulf of Bothnia, Gulf of Finland and Baltic Sea could be a significant source for the emission of
756 iodine precursors and DMS. The gases produced by these emissions further oxidize in the atmosphere
757 to form IA and SA, which can be detected by mass spectrometric methods. Interestingly, during
758 marine air mass intrusion with higher residence time over the algal blooms, the gaseous precursors
759 formed from the biological emissions possibly exceeded the gaseous precursors sourced from

760 anthropogenic emissions at the measurement site. In fact, an overall higher impact of biogenic
761 emissions was noted in this semi-urban site particularly during end of July and mid-August when the
762 bloom intensity decreases and the cyanobacteria/macroalgae start to decay and die (while being
763 exposed to sunlight) and consequently produce more emissions (biogenic SA and IA). 2) Moreover,
764 the meteorological conditions like wind direction and possibly wind speed were identified as the most
765 important parameters influencing the precursor vapor concentration reaching the measurement site
766 and thus determining if NPF occurred. Further we also infer that that the wind direction played an
767 important role in determining the particle concentrations at the study site. Our study reports, that
768 when the air mass travelled over the land with higher residence time over the urban areas, it was
769 enriched with SA and organics from proximal-local sources leading to the occurrence of regional and
770 local events (30 June 2019 and 30 July 2019). In contrast, when the air mass travelled over the water
771 bodies, with higher residence times over the cyanobacterial/algal blooms, the air mass was enriched
772 with biogenic SA and/or IA initiating a burst/spike event at the measurement site (11, 14, 15 August
773 2019). This observation is comparable to other coastal sites like Mace Head, although the NPF events
774 are much stronger in Mace Head, since the measurement site is just at the coast with intensive low
775 tide-high tide periods. 3) The formation rates of 1.5 nm particle and ions suggest that both IA-driven
776 and SA-driven NPF events were neutral nucleation events. 4) The type of phytoplankton species,
777 intensity of the bloom and distance of the bloom from the experimental site is speculated to play an
778 important role in determining the concentrations of precursor gases and thus influence the duration
779 and type of NPF. The IA driven nucleation occurred when the air mass travelled from over the Baltic
780 Sea region, where the coasts are dominated by several species of macroalgae, including *F.*
781 *vesiculosus*. The SA rich burst events occurred when air mass travelled over the Gulf of Bothnia
782 which was mainly dominated by the cyanobacteria species *Aphanizomenon*. 5) Burst/spike events,
783 connected to high IA concentrations, likely led to fast growth of particles potentially to CCN sizes.
784 The role of stabilizing the IA clusters by SA and ammonia in a semi-urban coastal place needs to be
785 further explored. The growth rate of particles was not fully explained by the SA, IA and MSA alone,
786 this applies especially for 3–7 nm or larger particles, indicating that organics might be playing a
787 critical role in the growth of particles in this semi-urban location. We have significantly high ambient
788 concentrations of HOMs in this study, although the detailed descriptions is beyond the scope of this
789 work.

790 The role of organics (HOMs) in the growth of particles is an active research question.
791 Exploring the sources and characterizing them during a bloom period, when the emission of biogenic
792 volatile organics increase with temperature, is crucial to understand the climate linkages of aerosol
793 formation. In order to resolve these links more quantitative studies are required, which aims to

794 understand the correlation between the quality and quantity of cyanobacterial blooms and the strength
795 of emissions of aerosol precursor vapors. More systematic studies, partitioning the influence of
796 pelagic cyanobacterial blooms and coastal macroalgae on new particle formations, would need to be
797 undertaken.

798

799 *Data availability*

800 Mass spectrometer data for SA, IA, MSA and HOMs are available at
801 <https://doi.org/10.5281/zenodo.6426198> . Neutral cluster and air ion spectrometer data related to this
802 article are available upon request to the corresponding author. Rest of the data are available for
803 download from <https://smear.avaa.csc.fi/download>.

804 *Supplement*

805 The supplement related to this article is available online at:

806 *Author contributions*

807 RCT,TJ and MS designed the experiment, MS, LB, NS, YJT, TC, YJ, JL, ML were involved in the
808 instrument installations and performed calibrations, RCT, collected, processed, analyzed and
809 interpreted the mass spectrometric data. TC, JS, JL, RCT and ML collected and processed the particle
810 data. RCT, LD and KL interpreted the particle data. LD, LB, LQ and XCH performed the calculations.
811 MS, RCT, TJ and MK conceptualized the idea of connecting marine biology and atmospheric
812 processes. AN improvised the marine biology section of the paper. CX carried out Flexpart analysis.
813 MM contributed to the satellite data procurement and its interpretation. All authors contributed
814 commented on the manuscript and improvised the data interpretation.

815

816 *Competing Interests*

817 At least one of the (co-)authors is a member of the editorial board of Atmospheric Chemistry and
818 Physics. The peer-review process was guided by an independent editor, and the authors also have no
819 other competing interests to declare.

820

821 *Acknowledgements*

822 We thank the ACTRIS CiGAS-UHEL calibration center for providing facility for CI-APi-TOF
823 calibration and INAR technical staff for support during the entire experiment. We also acknowledge
824 Finnish Meteorological Institute for the provision of the wave height data in used this study through
825 the website <https://en.ilmatieteenlaitos.fi/wave-height>. We humbly acknowledge the useful
826 discussion and data reference obtained from Finnish Environmental Institute. . The authors gratefully

827 acknowledge the NOAA Air Resources Laboratory (ARL) for the provision of the HYSPLIT
828 transport and dispersion model and/or READY website (<https://www.ready.noaa.gov>) used in this
829 publication.

830

831 Financial support: This work was supported by the European Research Council (ERC) under the
832 European Union's Horizon 2020 research and innovation programme (GASPARCON, grant
833 agreement no. 714621) and by the Finnish Academy (grant agreement no. 334514). We also
834 acknowledge Jane and Aatos Erkkö Foundation, ERC ATM-GTP, Flagship ACCC and Aerosols,
835 clouds and trace gases infrastructure (ACTRIS) for funding support

836

837 **References**

838 Allan, J. D., Williams, P. I., Najera, J., Whitehead, J. D., Flynn, M. J., Taylor, J. W., Liu, D., Darbyshire, E.,
839 Carpenter, L. J., Chance, R., Andrews, S. J., Hackenberg, S. C. and McFiggans, G.: Iodine observed in
840 new particle formation events in the Arctic atmosphere during ACCACIA, *Atmos. Chem. Phys.*, 15(10),
841 5599–5609, doi:10.5194/acp-15-5599-2015, 2015.

842 Almeida, J., Schobesberger, S., Kürten, A., Ortega, I. K., Kupiainen-Määttä, O., Praplan, A. P., Adamov, A.,
843 Amorim, A., Bianchi, F., Breitenlechner, M., David, A., Dommen, J., Donahue, N. M., Downard, A.,
844 Dunne, E., Duplissy, J., Ehrhart, S., Flagan, R. C., Franchin, A., Guida, R., Hakala, J., Hansel, A.,
845 Heinritzi, M., Henschel, H., Jokinen, T., Junninen, H., Kajos, M., Kangasluoma, J., Keskinen, H., Kupc,
846 A., Kurtén, T., Kvashin, A. N., Laaksonen, A., Lehtipalo, K., Leiminger, M., Leppä, J., Loukonen, V.,
847 Makhmutov, V., Mathot, S., McGrath, M. J., Nieminen, T., Olenius, T., Onnela, A., Petäjä, T.,
848 Riccobono, F., Riipinen, I., Rissanen, M., Rondo, L., Ruuskanen, T., Santos, F. D., Sarnela, N.,
849 Schallhart, S., Schnitzhofer, R., Seinfeld, J. H., Simon, M., Sipilä, M., Stozhkov, Y., Stratmann, F.,
850 Tomé, A., Tröstl, J., Tsagkogeorgas, G., Vaattovaara, P., Viisanen, Y., Virtanen, A., Vrtala, A., Wagner,
851 P. E., Weingartner, E., Wex, H., Williamson, C., Wimmer, D., Ye, P., Yli-Juuti, T., Carslaw, K. S.,
852 Kulmala, M., Curtius, J., Baltensperger, U., Worsnop, D. R., Vehkamäki, H. and Kirkby, J.: Molecular
853 understanding of sulphuric acid-amine particle nucleation in the atmosphere, *Nature*, 502(7471), 359–
854 363, doi:10.1038/nature12663, 2013.

855 Andersen, J. H., Carstensen, J., Conley, D. J., Dromph, K., Fleming-Lehtinen, V., Gustafsson, B. G., Josefson,
856 A. B., Norkko, A., Villnäs, A. and Murray, C.: Long-term temporal and spatial trends in eutrophication
857 status of the Baltic Sea, *Biol. Rev.*, doi:10.1111/brv.12221, 2017.

858 Ar Gall, E., Küpper, F. C. and Kloareg, B.: A survey of iodine content in *Laminaria digitata*, *Bot. Mar.*,
859 doi:10.1515/BOT.2004.004, 2004.

860 Artaxo, P., Rizzo, L. V., Brito, J. F., Barbosa, H. M. J., Arana, A., Sena, E. T., Cirino, G. G., Bastos, W.,
861 Martin, S. T. and Andreae, M. O.: Atmospheric aerosols in Amazonia and land use change: From natural
862 biogenic to biomass burning conditions, *Faraday Discuss.*, 165, 203–235, doi:10.1039/c3fd00052d,

863 2013.

864 Attard, K. M., Rodil, I. F., Berg, P., Norkko, J., Norkko, A. and Glud, R. N.: Seasonal metabolism and carbon
865 export potential of a key coastal habitat: The perennial canopy-forming macroalga *Fucus vesiculosus*,
866 *Limnol. Oceanogr.*, doi:10.1002/lno.11026, 2019.

867 Baalbaki, R., Pikridas, M., Jokinen, T., Laurila, T., Dada, L., Bezantakos, S., Ahonen, L., Neitola, K., Maisser,
868 A., Bimenyimana, E., Christodoulou, A., Unga, F., Savvides, C., Lehtipalo, K., Kangasluoma, J.,
869 Biskos, G., Petäjä, T., Kerminen, V. M., Sciare, J. and Kulmala, M.: Towards understanding the
870 characteristics of new particle formation in the Eastern Mediterranean, *Atmos. Chem. Phys.*,
871 doi:10.5194/acp-21-9223-2021, 2021.

872 Baccarini, A., Karlsson, L., Dommen, J., Duplessis, P., Vüllers, J., Brooks, I. M., Saiz-Lopez, A., Salter, M.,
873 Tjernström, M., Baltensperger, U., Zieger, P. and Schmale, J.: Frequent new particle formation over the
874 high Arctic pack ice by enhanced iodine emissions, *Nat. Commun.*, doi:10.1038/s41467-020-18551-0,
875 2020.

876 Bates, T.S., Lamb, B.K., Guenther, A., Dignon, J. and Stoiber, R.E.: Sulfur emissions to the atmosphere from
877 natural sources., *J Atmos Chem.*, 14, 315–337, <https://doi.org/10.1007/BF00115242>, 1992. Beck, L. J.,
878 Sarnela, N., Junninen, H., Hoppe, C. J. M., Garmash, O., Bianchi, F., Riva, M., Rose, C., Peräkylä, O.,
879 Wimmer, D., Kausiala, O., Jokinen, T., Ahonen, L., Mikkilä, J., Hakala, J., He, X. C., Kontkanen, J.,
880 Wolf, K. K. E., Cappelletti, D., Mazzola, M., Traversi, R., Petroselli, C., Viola, A. P., Vitale, V., Lange,
881 R., Massling, A., Nøjgaard, J. K., Krejci, R., Karlsson, L., Zieger, P., Jang, S., Lee, K., Vakkari, V.,
882 Lampilahti, J., Thakur, R. C., Leino, K., Kangasluoma, J., Duplissy, E. M., Siivola, E., Marbouti, M.,
883 Tham, Y. J., Saiz-Lopez, A., Petäjä, T., Ehn, M., Worsnop, D. R., Skov, H., Kulmala, M., Kerminen,
884 V. M. and Sipilä, M.: Differing Mechanisms of New Particle Formation at Two Arctic Sites, *Geophys.*
885 *Res. Lett.*, doi:10.1029/2020GL091334, 2021.

886 Benson, D. R., Young, L. H., Kameel, F. R. and Lee, S. H.: Laboratory-measured nucleation rates of sulfuric
887 acid and water binary homogeneous nucleation from the SO₂ + OH reaction, *Geophys. Res. Lett.*,
888 35(11), 1–6, doi:10.1029/2008GL033387, 2008.

889 Bergman, T., Laaksonen, A., Korhonen, H., Malila, J., Dunne, E. M., Mielonen, T., Lehtinen, K. E. J., Kühn,
890 T., Arola, A. and Kokkola, H.: Geographical and diurnal features of amine-enhanced boundary layer
891 nucleation, *J. Geophys. Res. Atmos.*, 120, 9606–9624, doi:10.1002/2015JD023181, 2015.

892 Berresheim, H., Elste, T., Tremmel, H. G., Allen, A. G., Hansson, H. C., Rosman, K., Dal Maso, M., Mäkelä,
893 J. M., Kulmala, M. and O’Dowd, C. D.: Gas-aerosol relationships of H₂SO₄, MSA, and OH:
894 Observations in the coastal marine boundary layer at Mace Head, Ireland, *J. Geophys. Res. Atmos.*,
895 107(19), 1–12, doi:10.1029/2000JD000229, 2002.

896 Bianchi, F., Tröstl, J., Junninen, H., Frege, C., Henne, S., Hoyle, C. R., Molteni, U., Herrmann, E., Adamov,
897 A., Bukowiecki, N., Chen, X., Duplissy, J., Gysel, M., Hutterli, M., Kangasluoma, J., Kontkanen, J.,
898 Kürten, A., Manninen, H. E., Münch, S., Peräkylä, O., Petäjä, T., Rondo, L., Williamson, C.,
899 Weingartner, E., Curtius, J., Worsnop, D. R., Kulmala, M., Dommen, J. and Baltensperger, U.: New

900 particle formation in the free troposphere: A question of chemistry and timing, *Science* (80-.),
901 352(6289), 1109–1112, doi:10.1126/science.aad5456, 2016.

902 Bianchi, F., Junninen, H., Bigi, A., Sinclair, V. A., Dada, L., Hoyle, C. R., Zha, Q., Yao, L., Ahonen, L. R.,
903 Bonasoni, P., Buenrostro Mazon, S., Hutterli, M., Laj, P., Lehtipalo, K., Kangasluoma, J., Kerminen,
904 V. M., Kontkanen, J., Marinoni, A., Mirme, S., Molteni, U., Petäjä, T., Riva, M., Rose, C., Sellegri, K.,
905 Yan, C., Worsnop, D. R., Kulmala, M., Baltensperger, U. and Dommen, J.: Biogenic particles formed
906 in the Himalaya as an important source of free tropospheric aerosols, *Nat. Geosci.*, doi:10.1038/s41561-
907 020-00661-5, 2020.

908 Bigg, E. K. and Turvey, D. E.: Sources of atmospheric particles over Australia, *Atmos. Environ.*, 12(8), 1643–
909 1655, doi:10.1016/0004-6981(78)90313-X, 1978.

910 Boy, M., Karl, T., Turnipseed, A., Mauldin, R. L., Kosciuch, E., Greenberg, J., Rathbone, J., Smith, J., Held,
911 A., Barsanti, K., Wehner, B., Bauer, S., Wiedensohler, A., Bonn, B., Kulmala, M. and Guenther, A.:
912 New particle formation in the front range of the Colorado Rocky Mountains, *Atmos. Chem. Phys.*, 8(6),
913 1577–1590, doi:10.5194/acp-8-1577-2008, 2008.

914 Buenrostro Mazon, S., Kontkanen, J., Manninen, H. E., Nieminen, T., Kerminen, V. M. and Kulmala, M.: A
915 long-term comparison of nighttime cluster events and daytime ion formation in a boreal forest, *Boreal
916 Environ. Res.*, 21(3–4), 242–261, 2016.

917 Cai, R. and Jiang, J.: A new balance formula to estimate new particle formation rate: Reevaluating the effect
918 of coagulation scavenging, *Atmos. Chem. Phys.*, 17(20), 12659–12675, doi:10.5194/acp-17-12659-
919 2017, 2017.

920 Carbone, M. S., Park Williams, A., Ambrose, A. R., Boot, C. M., Bradley, E. S., Dawson, T. E., Schaeffer,
921 S. M., Schimel, J. P. and Still, C. J.: Cloud shading and fog drip influence the metabolism of a coastal
922 pine ecosystem *Global Change Biol.*, 19, 484–97, 2013.

923 Chan, T., Cai, R., Ahonen, L. R., Liu, Y., Zhou, Y., Vanhanen, J., Dada, L., Chao, Y., Liu, Y., Wang, L.,
924 Kulmala, M. and Kangasluoma, J.: Assessment of particle size magnifier inversion methods to obtain
925 the particle size distribution from atmospheric measurements, *Atmos. Meas. Tech.*, 13(9), 4885–4898,
926 doi:10.5194/amt-13-4885-2020, 2020.

927 Chen, D., Wang, W., Li, D. and Wang, W.: Atmospheric implication of synergy in methanesulfonic acid-base
928 trimers: A theoretical investigation, *RSC Adv.*, 10(9), 5173–5182, doi:10.1039/c9ra08760e, 2020.

929 Chen, H., Ezell, M. J., Arquero, K. D., Varner, M. E., Dawson, M. L., Gerber, R. B. and Finlayson-Pitts, B. J.:
930 New particle formation and growth from methanesulfonic acid, trimethylamine and water, *Phys. Chem.
931 Chem. Phys.*, 17(20), 13699–13709, doi:10.1039/c5cp00838g, 2015.

932 Chen, H., Varner, M. E., Gerber, R. B. and Finlayson-Pitts, B. J.: Reactions of Methanesulfonic Acid with
933 Amines and Ammonia as a Source of New Particles in Air, *J. Phys. Chem. B*, 120(8), 1526–1536,
934 doi:10.1021/acs.jpccb.5b07433, 2016.

935 Croft, B., Martin, R. V., Richard Leaitch, W., Tunved, P., Breider, T. J., D’Andrea, S. D. and Pierce, J. R.:
936 Processes controlling the annual cycle of Arctic aerosol number and size distributions, *Atmos. Chem.*

937 Phys., 16(6), 3665–3682, doi:10.5194/acp-16-3665-2016, 2016.

938 Dada, L., Paasonen, P., Nieminen, T., Buenrostro Mazon, S., Kontkanen, J., Peräkylä, O., Lehtipalo, K.,
939 Hussein, T., Petäjä, T., Kerminen, V. M., Bäck, J. and Kulmala, M.: Long-term analysis of clear-sky
940 new particle formation events and nonevents in Hyytiälä, *Atmos. Chem. Phys.*, doi:10.5194/acp-17-
941 6227-2017, 2017.

942 Dada, L., Chellapermal, R., Buenrostro Mazon, S., Paasonen, P., Lampilahti, J., E Manninen, H., Junninen,
943 H., Petäjä, T., Kerminen, V. M. and Kulmala, M.: Refined classification and characterization of
944 atmospheric new-particle formation events using air ions, *Atmos. Chem. Phys.*, 18(24), 17883–17893,
945 doi:10.5194/acp-18-17883-2018, 2018.

946 Dada, L., Ylivinkka, I., Baalbaki, R., Li, C., Guo, Y., Yan, C., Yao, L., Sarnela, N., Jokinen, T., Daellenbach,
947 K. R., Yin, R., Deng, C., Chu, B., Nieminen, T., Wang, Y., Lin, Z., Thakur, R. C., Kontkanen, J.,
948 Stolzenburg, D., Sipilä, M., Hussein, T., Paasonen, P., Bianchi, F., Salma, I., Weidinger, T., Pikridas,
949 M., Sciare, J., Jiang, J., Liu, Y., Petäjä, T., Kerminen, V. M. and Kulmala, M.: Sources and sinks driving
950 sulfuric acid concentrations in contrasting environments: Implications on proxy calculations, *Atmos.*
951 *Chem. Phys.*, doi:10.5194/acp-20-11747-2020, 2020.

952 Dal Maso, M., Kulmala, M., Riipinen, I., Wagner, R., Hussein, T., Aalto, P. P. and Lehtinen, K. E. J.:
953 Formation and growth of fresh atmospheric aerosols: Eight years of aerosol size distribution data from
954 SMEAR II, Hyytiälä, Finland, *Boreal Environ. Res.*, 10(5), 323–336, 2005.

955 Deng, C., Fu, Y., Dada, L., Yan, C., Cai, R., Yang, D., Zhou, Y., Yin, R., Lu, Y., Li, X., Qiao, X., Fan, X.,
956 Nie, W., Kontkanen, J., Kangasluoma, J., Chu, B., Ding, A., Kerminen, V. M., Paasonen, P., Worsnop,
957 D. R., Bianchi, F., Liu, Y., Zheng, J., Wang, L., Kulmala, M. and Jiang, J.: Seasonal characteristics of
958 new particle formation and growth in urban Beijing, *Environ. Sci. Technol.*, 54(14), 8547–8557,
959 doi:10.1021/acs.est.0c00808, 2020.

960 Dowd, C. D. O., Lowe, J. A., Smith, M. H., Davison, B., Hewitt, C. N. and Harrison, R. M.: Biogenic sulphur
961 emissions and inferred non-sea-salt-sulphate particularly during Events of new particle formation were
962 Instrumentation and Cruise Summary, *Atlantic*, 102(DII), 1997.

963 Du, W., Dada, L., Zhao, J., Chen, X., Daellenbach, K. R., Xie, C., Wang, W., He, Y., Cai, J., Yao, L., Zhang,
964 Y., Wang, Q., Xu, W., Wang, Y., Tang, G., Cheng, X., Kokkonen, T. V., Zhou, W., Yan, C., Chu, B.,
965 Zha, Q., Hakala, S., Kurppa, M., Järvi, L., Liu, Y., Li, Z., Ge, M., Fu, P., Nie, W., Bianchi, F., Petäjä,
966 T., Paasonen, P., Wang, Z., Worsnop, D. R., Kerminen, V. M., Kulmala, M. and Sun, Y.: A 3D study
967 on the amplification of regional haze and particle growth by local emissions, *npj Clim. Atmos. Sci.*,
968 doi:10.1038/s41612-020-00156-5, 2021.

969 Duplissy, J., Merikanto, J., Franchin, A., Tsagkogeorgas, G., Kangasluoma, J., Wimmer, D., Vuollekoski, H.,
970 Schobesberger, S., Lehtipalo, K., Flagan, R. C., Brus, D., Donahue, N. M., Vehkamäki, H., Almeida, J.,
971 Amorim, A., Barmet, P., Bianchi, F., Breitenlechner, M., Dunne, E. M., Guida, R., Henschel, H.,
972 Junninen, H., Kirkby, J., Kürten, A., Kupc, A., Määttänen, A., Makhmutov, V., Mathot, S., Nieminen,
973 T., Onnela, A., Praplan, A. P., Riccobono, F., Rondo, L., Steiner, G., Tome, A., Walther, H.,

974 Baltensperger, U., Carslaw, K. S., Dommen, J., Hansel, A., Petäjä, T., Sipilä, M., Stratmann, F., Vrtala,
975 A., Wagner, P. E., Worsnop, D. R., Curtius, J. and Kulmala, M.: *Journal of Geophysical Research :
976 Atmospheres*, , 1752–1775, doi:10.1002/2015JD023538.Effect, 2016.

977 Eisele, Fred L; Tanner, D. : Measurement of the gas phase concentration of H₂SO₄ and Methane sulphonic
978 acid and estimates of H₂SO₄ production and Loss in Atmosphere, , 98(93), 9001–9010, 1993.

979 Eisele, F. L., Lovejoy, E. R., Kosciuch, E., Moore, K. F., Mauldin, I. L., Smith, J. N., McMurry, P. H. and
980 Iida, K.: Negative atmospheric ions and their potential role in ion-induced nucleation, *J. Geophys. Res.*
981 *Atmos.*, 111(4), doi:10.1029/2005JD006568, 2006.

982 Ehn, M., Thornton, J. A., Kleist, E., Sipilä, M., Junninen, H., Pullinen, I., Springer, M., Rubach, F.,
983 Tillmann, R., Lee, B., Lopez-Hilfiker, F., Andres, S., Acir, I.-H. H., Rissanen, M., Jokinen, T.,
984 Schobesberger, S., Kangasluoma, J., Kontkanen, J., Nieminen, T., Kurtén, T., Nielsen, L. B.,
985 Jørgensen, S., Kjaergaard, H. G., Canagaratna, M., Maso, M. D., Berndt, T., Petäjä, T., Wahner, A.,
986 Kerminen, V.-M. M., Kulmala, M., Worsnop, D. R., Wildt, J. and Mentel, T. F.: A large source of
987 low-volatility secondary organic aerosol, *Nature*, 506(7489), 476–479, doi:10.1038/nature13032,
988 2014.

989 Emery, N. C., D'Antonio, C. M. and Still, C. J.: Fog and live fuel moisture in coastal California shrublands
990 *Ecosphere*, 9, e02167, <https://doi.org/10.1002/ecs2.2167> ,2018.

991 Fiedler, V., Dal Maso, M., Boy, M., Aufmhoff, H., Hoffmann, J., Schuck, T., Birmili, W., Hanke, M., Uecker,
992 J., Arnold, F. and Kulmala, M.: The contribution of sulphuric acid to atmospheric particle formation and
993 growth: A comparison between boundary layers in Northern and Central Europe, *Atmos. Chem. Phys.*,
994 5(7), 1773–1785, doi:10.5194/acp-5-1773-2005, 2005.

995 Flanagan, R. J., Geever, M. and O'Dowd, C. D.: Direct measurements of new-particle fluxes in the coastal
996 environment, *Environ. Chem.*, 2(4), 256–259, doi:10.1071/EN05069, 2005.

997 Funkey, C. P., Conley, D. J., Reuss, N. S., Humborg, C., Jilbert, T. and Slomp, C. P.: Hypoxia sustains
998 cyanobacteria blooms in the Baltic Sea, *Environ. Sci. Technol.*, doi:10.1021/es404395a, 2014.

999 Glasoe, W. A., Volz, K., Panta, B., Freshour, N., Bachman, R., Hanson, D. R., McMurry, P. H. and Jen, C.:
1000 Sulphuric acid nucleation: An experimental study of the effect of seven bases, *J. Geophys. Res.*,
1001 doi:10.1002/2014JD022730, 2015.He, X. C., Iyer, S., Sipilä, M., Ylisirniö, A., Peltola, M., Kontkanen,
1002 J., Baalbaki, R., Simon, M., Kürten, A., Tham, Y. J., Pesonen, J., Ahonen, L. R., Amanatidis, S.,
1003 Amorim, A., Baccharini, A., Beck, L., Bianchi, F., Brilke, S., Chen, D., Chiu, R., Curtius, J., Dada, L.,
1004 Dias, A., Dommen, J., Donahue, N. M., Duplissy, J., El Haddad, I., Finkenzeller, H., Fischer, L.,
1005 Heinritzi, M., Hofbauer, V., Kangasluoma, J., Kim, C., Koenig, T. K., Kubečka, J., Kvashnin, A.,
1006 Lamkaddam, H., Lee, C. P., Leiminger, M., Li, Z., Makhmutov, V., Xiao, M., Marten, R., Nie, W.,
1007 Onnela, A., Partoll, E., Petäjä, T., Salo, V. T., Schuchmann, S., Steiner, G., Stolzenburg, D., Stozhkov,
1008 Y., Tauber, C., Tomé, A., Väisänen, O., Vazquez-Pufleau, M., Volkamer, R., Wagner, A. C., Wang, M.,
1009 Wang, Y., Wimmer, D., Winkler, P. M., Worsnop, D. R., Wu, Y., Yan, C., Ye, Q., Lehtinen, K.,
1010 Nieminen, T., Manninen, H. E., Rissanen, M., Schobesberger, S., Lehtipalo, K., Baltensperger, U.,

- 1011 Hansel, A., Kerminen, V. M., Flagan, R. C., Kirkby, J., Kurtén, T. and Kulmala, M.: Determination of
1012 the collision rate coefficient between charged iodine acid clusters and iodine acid using the appearance
1013 time method, *Aerosol Sci. Technol.*, doi:10.1080/02786826.2020.1839013, 2021a.
- 1014 He, X. C., Tham, Y. J., Dada, L., Wang, M., Finkenzeller, H., Stolzenburg, D., Iyer, S., Simon, M., Kürten,
1015 A., Shen, J., Rörup, B., Rissanen, M., Schobesberger, S., Baalbaki, R., Wang, D. S., Koenig, T. K.,
1016 Jokinen, T., Sarnela, N., Beck, L. J., Almeida, J., Amanatidis, S., Amorim, A., Ataei, F., Baccarini, A.,
1017 Bertozzi, B., Bianchi, F., Brilke, S., Caudillo, L., Chen, D., Chiu, R., Chu, B., Dias, A., Ding, A.,
1018 Dommen, J., Duplissy, J., Haddad, I. El, Carracedo, L. G., Granzin, M., Hansel, A., Heinritzi, M.,
1019 Hofbauer, V., Junninen, H., Kangasluoma, J., Kempainen, D., Kim, C., Kong, W., Krechmer, J. E.,
1020 Kvashin, A., Laitinen, T., Lamkaddam, H., Lee, C. P., Lehtipalo, K., Leiminger, M., Li, Z., Makhmutov,
1021 V., Manninen, H. E., Marie, G., Marten, R., Mathot, S., Mauldin, R. L., Mentler, B., Möhler, O., Müller,
1022 T., Nie, W., Onnela, A., Petäjä, T., Pfeifer, J., Philippov, M., Ranjithkumar, A., Saiz-Lopez, A., Salma,
1023 I., Scholz, W., Schuchmann, S., Schulze, B., Steiner, G., Stozhkov, Y., Tauber, C., Tomé, A., Thakur,
1024 R. C., Väisänen, O., Vazquez-Pufleau, M., Wagner, A. C., Wang, Y., Weber, S. K., Winkler, P. M., Wu,
1025 Y., Xiao, M., Yan, C., Ye, Q., Ylisirniö, A., Zauner-Wieczorek, M., Zha, Q., Zhou, P., Flagan, R. C.,
1026 Curtius, J., Baltensperger, U., Kulmala, M., Kerminen, V. M., Kurtén, T., et al.: Role of iodine oxoacids
1027 in atmospheric aerosol nucleation, *Science* (80-.), doi:10.1126/science.abe0298, 2021b.
- 1028 Hoffmann, E. H., Tilgner, A., Schrödner, R., Bräuer, P., Wolke, R. and Herrmann, H.: An advanced modeling
1029 study on the impacts and atmospheric implications of multiphase dimethyl sulfide chemistry, *Proc. Natl.*
1030 *Acad. Sci. U. S. A.*, doi:10.1073/pnas.1606320113, 2016.
- 1031 Huang, R.-J., Seitz, K., Buxmann, J., Poehler, D., Hornsby, K. E., Carpenter, L. J., Platt, U. and Hoffmann,
1032 T.: In situ measurements of molecular iodine in the marine boundary layer: the link to macroalgae and
1033 the implications for O₃, IO, OIO and NO_x, *Atmos.*
1034 *Chem. Phys. Discuss.*, 10(1), 361–390, doi:10.5194/acpd-10-361-2010, 2010.
- 1035 Huang, R. J., Thorenz, U. R., Kundel, M., Venables, D. S., Ceburnis, D., Ho, K. F., Chen, J., Vogel, A. L.,
1036 Küpper, F. C., Smyth, P. P. A., Nitschke, U., Stengel, D. B., Berresheim, H., O’Dowd, C. D. and
1037 Hoffmann, T.: The seaweeds *Fucus vesiculosus* and *Ascophyllum nodosum* are significant contributors
1038 to coastal iodine emissions, *Atmos. Chem. Phys.*, 13(10), 5255–5264, doi:10.5194/acp-13-5255-2013,
1039 2013.
- 1040 Humborg, C., Geibel, M.C., Sun, X., McCrackin, M, Mörth, C-M., Stranne. C., Jakobsson, M., Gustafsson,
1041 B., Sokolov, A., Norkko, A. and Norkko, J.: High Emissions of Carbon Dioxide and Methane From the
1042 Coastal Baltic Sea at the End of a Summer Heat Wave. *Front. Mar. Sci.* 6, [https://doi.org/10.3389/
1043 fmars.2019.00493](https://doi.org/10.3389/fmars.2019.00493), 2019.
- 1044 Iida, K., Stolzenburg, M. R., McMurry, P. H. and Smith, J. N.: Estimating nanoparticle growth rates from size-
1045 dependent charged fractions: Analysis of new particle formation events in Mexico City, *J. Geophys.*
1046 *Res. Atmos.*, 113(5), 1–15, doi:10.1029/2007JD009260, 2008.
- 1047 Jang, E., Park, K. T., Jun Yoon, Y., Kim, T. W., Hong, S. B., Becagli, S., Traversi, R., Kim, J. and Gim, Y.:

1048 New particle formation events observed at the King Sejong Station, Antarctic Peninsula - Part 2: Link
 1049 with the oceanic biological activities, *Atmos. Chem. Phys.*, 19(11), 7595–7608, doi:10.5194/acp-19-
 1050 7595-2019, 2019.

1051 Jokinen, T., Sipilä, M., Junninen, H., Ehn, M., Lönn, G., Hakala, J., Petäjä, T., Mauldin, R. L., Kulmala, M.
 1052 and Worsnop, D. R.: Atmospheric sulphuric acid and neutral cluster measurements using CI-APi-TOF,
 1053 *Atmos. Chem. Phys.*, 12(9), 4117–4125, doi:10.5194/acp-12-4117-2012, 2012.

1054 Jokinen, T., Sipilä, M., Kontkanen, J., Vakkari, V., Tisler, P., Duplissy, E. M., Junninen, H., Kangasluoma, J.,
 1055 Manninen, H. E., Petäjä, T., Kulmala, M., Worsnop, D. R., Kirkby, J., Virkkula, A. and Kerminen, V.
 1056 M.: Ion-induced sulfuric acid–ammonia nucleation drives particle formation in coastal Antarctica, *Sci.*
 1057 *Adv.*, 4(11), 1–7, doi:10.1126/sciadv.aat9744, 2018.

1058 Jokinen, T., Kontkanen, J., Lehtipalo, K. et al. Solar eclipse demonstrating the importance of photochemistry
 1059 in new particle formation. *Sci Rep* 7, 45707, <https://doi.org/10.1038/srep45707>, 2017. Junninen, H.,
 1060 Ehn, M., Petäjä, T., Luosujärvi, L., Kotiaho, T., Kostianen, R., Rohner, U., Gonin, M., Fuhrer, K.,
 1061 Kulmala, M. and Worsnop, D. R.: A high-resolution mass spectrometer to measure atmospheric ion
 1062 composition, *Atmos. Meas. Tech. Discuss.*, 3(1), 599–636, doi:10.5194/amtd-3-599-2010, 2010.

1063 Kahru, M. and Elmgren, R.: Multidecadal time series of satellite-detected accumulations of cyanobacteria in
 1064 the Baltic Sea, *Biogeosciences*, doi:10.5194/bg-11-3619-2014, 2014.

1065 Kautsky, L. and Kautsky, N.: The Baltic Sea, including Bothnian Sea and Bothnian Bay, *Seas Millenn. - an*
 1066 *Environ. Eval.* - Vol. 1, 2000.

1067 Keller, M. D., Bellows, W. K. and Guillard, R. R. L.: Dimethyl Sulfide Production in Marine Phytoplankton.,
 1068 1989.

1069 Kettle, A. J. and Andreae, M. O.: Flux of dimethylsulfide from the oceans: A comparison of updated data sets
 1070 and flux models, *J. Geophys. Res. Atmos.*, doi:10.1029/2000JD900252, 2000.

1071 Kirkby, J., Curtius, J., Almeida, J., Dunne, E., Duplissy, J., Ehrhart, S., Franchin, A., Gagné, S., Ickes, L.,
 1072 Kürten, A., Kupc, A., Metzger, A., Riccobono, F., Rondo, L., Schobesberger, S., Tsagkogeorgas, G.,
 1073 Wimmer, D., Amorim, A., Bianchi, F., Breitenlechner, M., David, A., Dommen, J., Downard, A., Ehn,
 1074 M., Flagan, R. C., Haider, S., Hansel, A., Hauser, D., Jud, W., Junninen, H., Kreissl, F., Kvashin, A.,
 1075 Laaksonen, A., Lehtipalo, K., Lima, J., Lovejoy, E. R., Makhmutov, V., Mathot, S., Mikkilä, J.,
 1076 Minginette, P., Mogo, S., Nieminen, T., Onnela, A., Pereira, P., Petäjä, T., Schnitzhofer, R., Seinfeld, J.
 1077 H., Sipilä, M., Stozhkov, Y., Stratmann, F., Tomé, A., Vanhanen, J., Viisanen, Y., Vrtala, A., Wagner,
 1078 P. E., Walther, H., Weingartner, E., Wex, H., Winkler, P. M., Carslaw, K. S., Worsnop, D. R.,
 1079 Baltensperger, U. and Kulmala, M.: Role of sulphuric acid, ammonia and galactic cosmic rays in
 1080 atmospheric aerosol nucleation, *Nature*, 476(7361), 429–435, doi:10.1038/nature10343, 2011.

1081 Kirkby, J., Duplissy, J., Sengupta, K., Frege, C., Gordon, H., Williamson, C., Heinritzi, M., Simon, M., Yan,
 1082 C., Almeida, J., Trostl, J., Nieminen, T., Ortega, I. K., Wagner, R., Adamov, A., Amorim, A.,
 1083 Bernhammer, A. K., Bianchi, F., Breitenlechner, M., Brilke, S., Chen, X., Craven, J., Dias, A., Ehrhart,
 1084 S., Flagan, R. C., Franchin, A., Fuchs, C., Guida, R., Hakala, J., Hoyle, C. R., Jokinen, T., Junninen, H.,

1085 Kangasluoma, J., Kim, J., Krapf, M., Kurten, A., Laaksonen, A., Lehtipalo, K., Makhmutov, V., Mathot,
1086 S., Molteni, U., Onnela, A., Perakyla, O., Piel, F., Petaja, T., Praplan, A. P., Pringle, K., Rap, A.,
1087 Richards, N. A. D., Riipinen, I., Rissanen, M. P., Rondo, L., Sarnela, N., Schobesberger, S., Scott, C.
1088 E., Seinfeld, J. H., Sipila, M., Steiner, G., Stozhkov, Y., Stratmann, F., Tomé, A., Virtanen, A., Vogel,
1089 A. L., Wagner, A. C., Wagner, P. E., Weingartner, E., Wimmer, D., Winkler, P. M., Ye, P., Zhang, X.,
1090 Hansel, A., Dommen, J., Donahue, N. M., Worsnop, D. R., Baltensperger, U., Kulmala, M., Carslaw,
1091 K. S. and Curtius, J.: Ion-induced nucleation of pure biogenic particles, *Nature*, 533(7604), 521–526,
1092 doi:10.1038/nature17953, 2016.

1093 Knutson, E. O. and Whitby, K. T.: Aerosol classification by electric mobility: apparatus, theory, and
1094 applications, *J. Aerosol Sci.*, 6(6), 443–451, doi:10.1016/0021-8502(75)90060-9, 1975.

1095 Knutson, E. O., Whitby, K. T., Fiedler, V., Dal Maso, M., Boy, M., Aufmhoff, H., Hoffmann, J., Schuck, T.,
1096 Birmili, W., Hanke, M., Uecker, J., Arnold, F., Kulmala, M., Petäjä, T., Nieminen, T., Sipilä, M.,
1097 Manninen, H. E., Lehtipalo, K., Dal Maso, M., Aalto, P. P., Junninen, H., Paasonen, P., Riipinen, I.,
1098 Lehtinen, K. E. J., Laaksonen, A., Kerminen, V. M., Croft, B., Martin, R. V., Richard Leitch, W.,
1099 Tunved, P., Breider, T. J., D’Andrea, S. D., Pierce, J. R., Glasoe, W. A., Volz, K., Panta, B., Freshour,
1100 N., Bachman, R., Hanson, D. R., McMurry, P. H., Jen, C., Suikkanen, S., Pulina, S., Engström-Öst, J.,
1101 Lehtiniemi, M., Lehtinen, S., Brutemark, A., Berresheim, H., Elste, T., Tremmel, H. G., Allen, A. G.,
1102 Hansson, H. C., Rosman, K., Dal Maso, M., Mäkelä, J. M., Kulmala, M., O’Dowd, C. D., Lehtinen, K.
1103 E. J., Kulmala, M., Manninen, H. E., Nieminen, T., Asmi, E., Gagné, S., Häkkinen, S., Lehtipalo, K.,
1104 Aalto, P. P., Vana, M., Mirme, A., Mirme, S., Hörrak, U., Plass-Dülmer, C., Stange, G., Kiss, G., Hoffer,
1105 A., Töro, N., Moerman, M., Henzing, B., De Leeuw, G., Brinkenberg, M., Kouvarakis, G. N.,
1106 Bougiatioti, A., Mihalopoulos, N., O’Dowd, C. D., Ceburnis, D., Arneth, A., Svenningsson, B.,
1107 Swietlicki, E., Tarozzi, L., Decesari, S., Facchini, M. C., Birmili, W., Sonntag, A., Wiedensohler, A.,
1108 Boulon, J., Sellegri, K., Laj, P., Gysel, M., Bukowiecki, N., Weingartner, E., et al.: Quantification of the
1109 volatility of secondary organic compounds in ultrafine particles during nucleation events, *Atmos. Chem.*
1110 *Phys.*, 10(4), 1–10, doi:10.1039/c9ra08760e, 2016.

1111 Kownacka, J., Calkiewicz, J. and Kornijów, R.: A turning point in the development of phytoplankton in the
1112 Vistula Lagoon (southern Baltic Sea) at the beginning of the 21st century, *Oceanologia*,
1113 doi:10.1016/j.oceano.2020.08.004, 2020.

1114 Kulmala, M., Toivonen, A., Mäkelä, J. M. and Laaksonen, A.: Analysis of the growth of nucleation mode
1115 particles observed in Boreal forest, *Tellus, Ser. B Chem. Phys. Meteorol.*,
1116 doi:10.3402/tellusb.v50i5.16229, 1998.

1117 Kulmala, M., Laakso, L., Lehtinen, K. E. J., Riipinen, I., Dal Maso, M., Anttila, T., Kerminen, V.-M., Hörrak,
1118 U., Vana, M. and Tammet, H.: Initial steps of aerosol growth, *Atmos. Chem. Phys.*, doi:10.5194/acp-4-
1119 2553-2004, 2004.

1120 Kulmala, M., Petäjä, T., Mönkkönen, P., Koponen, I. K., Dal Maso, M., Aalto, P. P., Lehtinen, K. E. J. and
1121 Kerminen, V. M.: On the growth nucleation mode particles: Source rates of condensable vapor in

1122 polluted and clean environments, *Atmos. Chem. Phys.*, 5(2), 409–416, doi:10.5194/acp-5-409-2005,
1123 2005.

1124 Kulmala, M., Petäjä, T., Nieminen, T., Sipilä, M., Manninen, H. E., Lehtipalo, K., Dal Maso, M., Aalto, P. P.,
1125 Junninen, H., Paasonen, P., Riipinen, I., Lehtinen, K. E. J., Laaksonen, A. and Kerminen, V. M.:
1126 Measurement of the nucleation of atmospheric aerosol particles, *Nat. Protoc.*, 7(9), 1651–1667,
1127 doi:10.1038/nprot.2012.091, 2012.

1128 Kulmala, M., Kontkanen, J., Junninen, H., Lehtipalo, K., Manninen, H. E., Nieminen, T., Petäjä, T., Sipilä,
1129 M., Schobesberger, S., Rantala, P., Franchin, A., Jokinen, T., Järvinen, E., Äijälä, M., Kangasluoma, J.,
1130 Hakala, J., Aalto, P. P., Paasonen, P., Mikkilä, J., Vanhanen, J., Aalto, J., Hakola, H., Makkonen, U.,
1131 Ruuskanen, T., Mauldin, R. L., Duplissy, J., Vehkamäki, H., Bäck, J., Kortelainen, A., Riipinen, I.,
1132 Kurtén, T., Johnston, M. V., Smith, J. N., Ehn, M., Mentel, T. F., Lehtinen, K. E. J., Laaksonen, A.,
1133 Kerminen, V. M. and Worsnop, D. R.: Direct observations of atmospheric aerosol nucleation, *Science*
1134 (80), 339(6122), 943–946, doi:10.1126/science.1227385, 2013.

1135 Kulmala, M., Petäjä, T., Kerminen, V. M., Kujansuu, J., Ruuskanen, T., Ding, A., Nie, W., Hu, M., Wang, Z.,
1136 Wu, Z., Wang, L. and Worsnop, D. R.: On secondary new particle formation in China, *Front. Environ.*
1137 *Sci. Eng.*, 10(5), 1–10, doi:10.1007/s11783-016-0850-1, 2016.

1138 Kulmala, M., Kerminen, V. M., Petäjä, T., Ding, A. J. and Wang, L.: Atmospheric gas-to-particle conversion:
1139 Why NPF events are observed in megacities?, *Faraday Discuss.*, 200, 271–288,
1140 doi:10.1039/c6fd00257a, 2017.

1141 Kuosa, H., Fleming-Lehtinen, V., Lehtinen, S., Lehtiniemi, M., Nygård, H., Raateoja, M., Raitaniemi, J.,
1142 Tuimala, J., Uusitalo, L. and Suikkanen, S.: A retrospective view of the development of the Gulf of
1143 Bothnia ecosystem, *J. Mar. Syst.*, 167, 78–92, doi:10.1016/j.jmarsys.2016.11.020, 2017.

1144 Küpper, F. C., Schweigert, N., Ar Gall, E., Legendre, J. M., Vilter, H. and Kloareg, B.: Iodine uptake in
1145 Laminariales involves extracellular, haloperoxidase-mediated oxidation of iodide, *Planta*,
1146 doi:10.1007/s004250050469, 1998.

1147 Kürten, A., Jokinen, T., Simon, M., Sipilä, M., Sarnela, N.,
1148 Junninen, H., Adamov, A., Almeida, J., Amorim, A., Bianchi, F., Breitenlechner, M., Dommen, J.,
1149 Donahue, N. M., Duplissy, J., Ehrhart, S., Flagan, R. C., Franchin, A., Hakala, J., Hansel, A., Heinritzi,
1150 M., Hutterli, M., Kangasluoma, J., Kirkby, J., Laaksonen, A., Lehtipalo, K., Leiminger, M.,
1151 Makhmutov, V., Mathot, S., Onnela, A., Petäjä, T., Praplan, A. P., Riccobono, F., Rissanen, M. P.,
1152 Rondo, L., Schobesberger, S., Seinfeld, J. H., Steiner, G., Tomé, A., Tröstl, J., Winkler, P. M.,
1153 Williamson, C., Wimmer, D., Ye, P., Baltensperger, U., Carslaw, K. S., Kulmala, M., Worsnop, D. R.
1154 and Curtius, J.: Neutral molecular cluster formation of sulfuric acid-dimethylamine observed in real
1155 time under atmospheric conditions, *Proc. Natl. Acad. Sci. U. S. A.*, 111(42), 15019–15024,
doi:10.1073/pnas.1404853111, 2014.

1156 Kürten, A., Münch, S., Rondo, L., Bianchi, F., Duplissy, J., Jokinen, T., Junninen, H., Sarnela, N.,
1157 Schobesberger, S., Simon, M., Sipilä, M., Almeida, J., Amorim, A., Dommen, J., Donahue, N. M.,
1158 Dunne, E. M., Flagan, R. C., Franchin, A., Kirkby, J., Kupc, A., Makhmutov, V., Petäjä, T., Praplan, A.

1159 P., Riccobono, F., Steiner, G., Tomé, A., Tsagkogeorgas, G., Wagner, P. E., Wimmer, D., Baltensperger,
1160 U., Kulmala, M., Worsnop, D. R. and Curtius, J.: Thermodynamics of the formation of sulfuric acid
1161 dimers in the binary (H₂SO₄-H₂O) and ternary (H₂SO₄-H₂O-NH₃) system, *Atmos. Chem. Phys.*,
1162 15(18), 10701–10721, doi:10.5194/acp-15-10701-2015, 2015.

1163 Kürten, A., Bianchi, F., Almeida, J., Kupiainen-Määttä, O., Dunne, E. M., Duplissy, J., Williamson, C.,
1164 Barmet, P., Breitenlechner, M., Dommen, J., Donahue, N. M., Flagan, R. C., Franchin, A., Gordon, H.,
1165 Hakala, J., Hansel, A., Heinritzi, M., Ickes, L., Jokinen, T., Kangasluoma, J., Kim, J., Kirkby, J., Kupc,
1166 A., Lehtipalo, K., Leiminger, M., Makhmutov, V., Onnela, A., Ortega, I. K., Petäjä, T., Praplan, A. P.,
1167 Riccobono, F., Rissanen, M. P., Rondo, L., Schnitzhofer, R., Schobesberger, S., Smith, J. N., Steiner,
1168 G., Stozhkov, Y., Tomé, A., Tröstl, J., Tsagkogeorgas, G., Wagner, P. E., Wimmer, D., Ye, P.,
1169 Baltensperger, U., Carslaw, K., Kulmala, M. and Curtius, J.: Experimental particle formation rates
1170 spanning tropospheric sulfuric acid and ammonia abundances, ion production rates, and temperatures,
1171 *J. Geophys. Res.*, doi:10.1002/2015JD023908, 2016.

1172 Kurten, T., Petäjä, T., Smith, J., Ortega, I. K., Sipilä, M., Junninen, H., Ehn, M., Vehkamäki, H., Mauldin,
1173 L., Worsnop, D. R. and Kulmala, M.: The effect of H₂SO₄ – amine clustering on chemical ionization
1174 mass spectrometry (CIMS) measurements of gas-phase sulfuric acid, *Atmos. Chem. Phys.*, 11, 3007–
1175 3019, doi:10.5194/acp-11-3007-2011, 2011.

1176 Kyrö, E. M., Väänänen, R., Kerminen, V. M., Virkkula, A., Petäjä, T., Asmi, A., Dal Maso, M., Nieminen, T.,
1177 Juhola, S., Shcherbinin, A., Riipinen, I., Lehtipalo, K., Keronen, P., Aalto, P. P., Hari, P. and Kulmala,
1178 M.: Trends in new particle formation in eastern Lapland, Finland: Effect of decreasing sulfur emissions
1179 from Kola Peninsula, *Atmos. Chem. Phys.*, 14(9), 4383–4396, doi:10.5194/acp-14-4383-2014, 2014.

1180 Lawson, D. M., Clamesha, R.E.S., Vanderplank, S., Gershunov, A. and Cayan, D.: Impacts and influences of
1181 coastal low clouds and fog on biodiversity in San Diego California’s Fourth Climate Change
1182 Assessment CCCA4-EXT-2018-010 69–89, [https://www.energy.ca.gov/sites/default/files/2019-](https://www.energy.ca.gov/sites/default/files/2019-12/Biodiversity_CCCA4-EXT-2018-010_ada_0.pdf)
1183 [12/Biodiversity_CCCA4-EXT-2018-010_ada_0.pdf](https://www.energy.ca.gov/sites/default/files/2019-12/Biodiversity_CCCA4-EXT-2018-010_ada_0.pdf), 2018.

1184 Lehtipalo, K., Yan, C., Dada, L., Bianchi, F., Xiao, M., Wagner, R., Stolzenburg, D., Ahonen, L. R., Amorim,
1185 A., Baccarini, A., Bauer, P. S., Baumgartner, B., Bergen, A., Bernhammer, A. K., Breitenlechner, M.,
1186 Brilke, S., Buchholz, A., Mazon, S. B., Chen, D., Chen, X., Dias, A., Dommen, J., Draper, D. C.,
1187 Duplissy, J., Ehn, M., Finkenzeller, H., Fischer, L., Frege, C., Fuchs, C., Garmash, O., Gordon, H.,
1188 Hakala, J., He, X., Heikkinen, L., Heinritzi, M., Helm, J. C., Hofbauer, V., Hoyle, C. R., Jokinen, T.,
1189 Kangasluoma, J., Kerminen, V.-M., Kim, C., Kirkby, J., Kontkanen, J., Kürten, A., Lawler, M. J., Mai,
1190 H., Mathot, S., Mauldin III, R. L., Molteni, U., Nichman, L., Nie, W., Nieminen, T., Ojdanic, A., Onnela,
1191 A., Passananti, M., Petäjä, T., Piel, F., Pospisilova, V., Quéléver, L. L. J., Rissanen, M. P., Rose, C.,
1192 Sarnela, N., Schallhart, S., Schuchmann, S., Sengupta, K., Simon, M., Sipilä, M., Tauber, C., Tomé,
1193 A., Tröstl, J., Väisänen, O., Vogel, A. L., Volkamer, R., Wagner, A. C., Wang, M., Weitz, L., Wimmer,
1194 D., Ye, P., Ylisirniö, A., Zha, Q., Carslaw, K. S., Curtius, J., Donahue, N. M., Flagan, R. C., Hansel, A.,
1195 Riipinen, I., Virtanen, A., Winkler, P. M., Baltensperger, U., Kulmala, M., and Worsnop, D. R.:

1196 Multicomponent new particle formation from sulfuric acid, ammonia, and 979 biogenic vapors, *Sci.*
1197 *Adv.*, 12, doi: 10.1126/sciadv.aau5363, 2018.

1198 Lehtipalo, K., Leppä, J., Kontkanen, J., Kangasluoma, J., Franchin, A., Wimmer, D., Schobesberger, S.,
1199 Junninen, H., Petäjä, T., Sipilä, M., Mikkilä, J., Vanhanen, J., Worsnop, D. R. and Kulmala, M.:
1200 Methods for determining particle size distribution and growth rates between 1 and 3 nm using the
1201 Particle Size Magnifier, *Boreal Environ. Res.*, 19(September), 215–236, 2014.

1202 Leino, K., Nieminen, T., Manninen, H. E., Petäjä, T., Kerminen, V. M. and Kulmala, M.: Intermediate ions as
1203 a strong indicator of new particle formation bursts in boreal forest, *Boreal Environ. Res.*, 21(3–4), 274–
1204 286, 2016.

1205 Mahajan, A. S., Oetjen, H., Saiz-Lopez, A., Lee, J. D., McFiggans, G. B. and Plane, J. M. C.: Reactive iodine
1206 species in a semi-polluted environment, *Geophys. Res. Lett.*, 36(16), 6–11,
1207 doi:10.1029/2009GL038018, 2009.

1208 Mahajan, A. S., Sorribas, M., Martín, J. C. G., MacDonald, S. M., Gil, M., Plane, J. M. C. and Saiz-Lopez, A.:
1209 Concurrent observations of atomic iodine, molecular iodine and ultrafine particles in a coastal
1210 environment, *Atmos. Chem. Phys.*, 11(6), 2545–2555, doi:10.5194/acp-11-2545-2011, 2011.

1211 Manninen, H. E., Nieminen, T., Asmi, E., Gagné, S., Häkkinen, S., Lehtipalo, K., Aalto, P., Vana, M., Mirme,
1212 A., Mirme, S., Hörrak, U., Plass-Dülmer, C., Stange, G., Kiss, G., Hoffer, A., Töro, N., Moerman, M.,
1213 Henzing, B., De Leeuw, G., Brinkenberg, M., Kouvarakis, G. N., Bougiatioti, A., Mihalopoulos, N.,
1214 O’Dowd, C., Ceburnis, D., Arneth, A., Svenningsson, B., Swietlicki, E., Tarozzi, L., Decesari, S.,
1215 Facchini, M. C., Birmili, W., Sonntag, A., Wiedensohler, A., Boulon, J., Sellegri, K., Laj, P., Gysel, M.,
1216 Bukowiecki, N., Weingartner, E., Wehrle, G., Laaksonen, A., Hamed, A., Joutsensaari, J., Petäjä, T.,
1217 Kerminen, V. M. and Kulmala, M.: EUCAARI ion spectrometer measurements at 12 European sites-
1218 analysis of new particle formation events, *Atmos. Chem. Phys.*, 10(16), 7907–7927, doi:10.5194/acp-
1219 10-7907-2010, 2010.

1220 Mauldin, R. L., Eisele, F. L., Kosciuch, E., Shetter, R., Lefer, B., Buhr, M., Chen, G., Wang, P. and Davis, D.:
1221 Oil] andjO (' D) , , 28(19), 3629–3632, 2001.

1222 McFiggans, G., Coe, H., Burgess, R., Allan, J., Cubison, M., Alfarra, M. R., Saunders, R., Saiz-Lopez, A.,
1223 Plane, J. M. C., Wevill, D. J., Carpenter, L. J., Rickard, A. R. and Monks, P. S.: Direct evidence for
1224 coastal iodine particles from *Laminaria* macroalgae - Linkage to emissions of molecular iodine, *Atmos.*
1225 *Chem. Phys.*, 4(3), 701–713, doi:10.5194/acp-4-701-2004, 2004.

1226 McFiggans, G., Bale, C. S. E., Ball, S. M., Beames, J. M., Bloss, W. J., Carpenter, L. J., Dorsey, J., Dunk, R.,
1227 Flynn, M. J., Furneaux, K. L., Gallagher, M. W., Heard, D. E., Hollingsworth, A. M., Hornsby, K.,
1228 Ingham, T., Jones, C. E., Jones, R. L., Kramer, L. J., Langridge, J. M., Leblanc, C., LeCrane, J. P., Lee,
1229 J. D., Leigh, R. J., Longley, I., Mahajan, A. S., Monks, P. S., Oetjen, H., Orr-Ewing, A. J., Plane, J. M.
1230 C., Potin, P., Shillings, A. J. L., Thomas, F., Von Glasow, R., Wada, R., Whalley, L. K. and Whitehead,
1231 J. D.: Iodine-mediated coastal particle formation: An overview of the Reactive Halogens in the Marine
1232 boundary layer (RHAMBLe) Roscoff coastal study, *Atmos. Chem. Phys.*, 10(6), 2975–2999,

1233 doi:10.5194/acp-10-2975-2010, 2010.

1234 Meixner, F. X. and Yang, W. X.: Biogenic emissions of nitric oxide and nitrous oxide from arid and semi-arid
1235 land, in *Dryland Ecohydrology.*, 2006.

1236 Mirme, S. and Mirme, A.: The mathematical principles and design of the NAIS - A spectrometer for the
1237 measurement of cluster ion and nanometer aerosol size distributions, *Atmos. Meas. Tech.*, 6(4), 1061–
1238 1071, doi:10.5194/amt-6-1061-2013, 2013.

1239 Nieminen, T., Asmi, A., Aalto, P. P., Keronen, P., Petäjä, T., Kulmala, M., Kerminen, V. M., Nieminen, T.
1240 and Dal Maso, M.: Trends in atmospheric new-particle formation: 16 years of observations in a boreal-
1241 forest environment, *Boreal Environ. Res.*, 19(September), 191–214, 2014.

1242 O’ Dowd, C. D., Jimenez, J. L., Bahreini, R., Flagan, R. C., Seinfeld, J. H., Hämerl, K., Pirjola, L., Kulmala,
1243 M. and Hoffmann, T.: Marine aerosol formation from biogenic iodine emissions, *Nature*, 417(6889),
1244 632–636, doi:10.1038/nature00775, 2002.

1245 Okuljar, M., Kuuluvainen, H., Kontkanen, J., Garmash, O., Olin, M., Niemi, J. V., Timonen, H., Kangasluoma,
1246 J., Tham, Y. J., Baalbaki, R., Sipilä, M., Salo, L., Lintusaari, H., Portin, H., Teinilä, K., Aurela, M., Dal
1247 Maso, M., Rönkkö, T., Petäjä, T. and Paasonen, P.: Measurement report: The influence of traffic and
1248 new particle formation on the size distribution of 1-800nm particles in Helsinki-a street canyon and an
1249 urban background station comparison, *Atmos. Chem. Phys.*, doi:10.5194/acp-21-9931-2021, 2021.

1250 Olin, M., Kuuluvainen, H., Aurela, M., Kalliokoski, J., Kuittinen, N., Isotalo, M., Timonen, H. J., Niemi, J.
1251 V., Rönkkö, T. and Dal Maso, M.: Traffic-originated nanocluster emission exceeds H₂SO₄-driven
1252 photochemical new particle formation in an urban area, *Atmos. Chem. Phys.*, 20(1), 1–13,
1253 doi:10.5194/acp-20-1-2020, 2020.

1254 Paasonen, P., Nieminen, T., Asmi, E., Manninen, H. E., Petäjä, T., Plass-Dülmer, C., Flentje, H., Birmili, W.,
1255 Wiedensohler, A., Hörrak, U., Metzger, A., Hamed, A., Laaksonen, A., Facchini, M. C., Kerminen, V.
1256 M. and Kulmala, M.: On the roles of sulphuric acid and low-volatility organic vapours in the initial steps
1257 of atmospheric new particle formation, *Atmos. Chem. Phys.*, 10(22), 11223–11242, doi:10.5194/acp-
1258 10-11223-2010, 2010.

1259 Peters, C., Pechtl, S., Stutz, J., Hebestreit, K., Hönninger, G., Heumann, K. G., Schwarz, A., Winterlik, J. and
1260 Platt, U.: Reactive and organic halogen species in three different European coastal environments, *Atmos.*
1261 *Chem. Phys.*, 5(12), 3357–3375, doi:10.5194/acp-5-3357-2005, 2005.

1262 Pierce, J. R., Riipinen, I., Kulmala, M., Ehn, M., Petäjä, T., Junninen, H., Worsnop, D. R. and Donahue, N.
1263 M.: Quantification of the volatility of secondary organic compounds in ultrafine particles during
1264 nucleation events, *Atmos. Chem. Phys.*, 11(17), 9019–9036, doi:10.5194/acp-11-9019-2011, 2011.

1265 Raso, A. R. W., Custard, K. D., May, N. W., Tanner, D., Newburn, M. K., Walker, L., Moore, R. J., Huey, L.
1266 G., Alexander, L., Shepson, P. B. and Pratt, K. A.: Active molecular iodine photochemistry in the Arctic,
1267 *Proc. Natl. Acad. Sci. U. S. A.*, 114(38), 10053–10058, doi:10.1073/pnas.1702803114, 2017.

1268 Riipinen, I., Yli-Juuti, T., Pierce, J. R., Petäjä, T., Worsnop, D. R., Kulmala, M. and Donahue, N. M.: The
1269 contribution of organics to atmospheric nanoparticle growth, *Nat. Geosci.*, 5(7), 453–458,

1270 doi:10.1038/ngeo1499, 2012.

1271 Riipinen, I., Yli-Juuti, T., Pierce, J. R., Petäjä, T., Worsnop, D. R., Kulmala, M. and Donahue, N. M.: The
1272 contribution of organics to atmospheric nanoparticle growth, *Nat. Geosci.*, doi:10.1038/ngeo1499,
1273 2012b.

1274 Rong, H., Liu, J., Zhang, Y., Du, L., Zhang, X. and Li, Z.: Nucleation mechanisms of iodic acid in clean and
1275 polluted coastal regions, *Chemosphere*, 253, 126743, doi:10.1016/j.chemosphere.2020.126743, 2020.

1276 Rose, C., Zha, Q., Dada, L., Yan, C., Lehtipalo, K., Junninen, H., Mazon, S. B., Jokinen, T., Sarnela, N., Sipilä,
1277 M., Petäjä, T., Kerminen, V. M., Bianchi, F. and Kulmala, M.: Observations of biogenic ion-induced
1278 cluster formation in the atmosphere, *Sci. Adv.*, 4(4), 1–11, doi:10.1126/sciadv.aar5218, 2018.

1279 Saiz-Lopez, A. and Plane, J. M. C.: Novel iodine chemistry in the marine boundary layer, *Geophys. Res. Lett.*,
1280 31(4), 1999–2002, doi:10.1029/2003GL019215, 2004.

1281 Saiz-Lopez, A., Plane, J. M. C., Baker, A. R., Carpenter, L. J., Von Glasow, R., Gómez Martín, J. C.,
1282 McFiggans, G. and Saunders, R. W.: Atmospheric chemistry of iodine, *Chem. Rev.*, 112(3), 1773–1804,
1283 doi:10.1021/cr200029u, 2012.

1284 Schade, G. W. and P. J. Crutzen.: Emission of aliphatic-amines from animal husbandry and their reactions:
1285 Potential source of N₂O and HCN, *J. Atmos. Chem.*, 22(3), 319–346, doi:10.1007/BF00696641, 1995.

1286 Schagerström, E., Forslund, H., Kautsky, L., Pärnoja, M. and Kotta, J.: Does thalli complexity and biomass
1287 affect the associated flora and fauna of two co-occurring *Fucus* species in the Baltic Sea?, *Estuar. Coast.*
1288 *Shelf Sci.*, doi:10.1016/j.ecss.2014.08.022, 2014.

1289 Sipilä, M., Sarnela, N., Jokinen, T., Junninen, H., Hakala, J., Rissanen, M. P., Praplan, A., Simon, M.,
1290 Kürten, A., Bianchi, F., Dommen, J., Curtius, J., Petäjä, T., and Worsnop, D. R.: Bisulfate – cluster
1291 based atmospheric pressure chemical ionization mass spectrometer for high-sensitivity (< 100 ppqV)
1292 detection of atmospheric dimethyl amine: proof-of-concept and first ambient data from boreal forest,
1293 *Atmos. Meas. Tech.*, 8, 4001–4011, <https://doi.org/10.5194/amt-8-4001-2015>, 2015.

1294 Sipilä, M., Berndt, T., Petäjä, T., Brus, D., Vanhanen, J., Stratmann, F., Patokoski, J., Mauldin, R. L.,
1295 Hyvärinen, A. P., Lihavainen, H. and Kulmala, M.: The role of sulfuric acid in atmospheric nucleation,
1296 *Science* (80-.), 327(5970), 1243–1246, doi:10.1126/science.1180315, 2010.

1297 Sipilä, M.: Insights Into Atmospheric Nucleation. [online] Available from:
1298 <https://helda.helsinki.fi/bitstream/handle/10138/154171/insights.pdf?sequence=1>, 2010.

1299 Sipilä, M., Sarnela, N., Jokinen, T., Henschel, H., Junninen, H., Kontkanen, J., Richters, S., Kangasluoma, J.,
1300 Franchin, A., Peräkylä, O., Rissanen, M. P., Ehn, M., Vehkamäki, H., Kurten, T., Berndt, T., Petäjä, T.,
1301 Worsnop, D., Ceburnis, D., Kerminen, V. M., Kulmala, M. and O’Dowd, C.: Molecular-scale evidence
1302 of aerosol particle formation via sequential addition of HIO₃, *Nature*, 537(7621), 532–534,
1303 doi:10.1038/nature19314, 2016.

1304 Steinke, M., Hodapp, B., Subhan, R., Bell, T. G. and Martin-Creuzburg, D.: Flux of the biogenic volatiles
1305 isoprene and dimethyl sulfide from an oligotrophic lake, *Sci. Rep.*, doi:10.1038/s41598-017-18923-5,
1306 2018.

1307 Stolzenburg, D., Stolzenburg, D., Simon, M., Ranjithkumar, A., Kürten, A., Lehtipalo, K., Lehtipalo, K.,
1308 Gordon, H., Ehrhart, S., Finkenzeller, H., Pichelstorfer, L., Nieminen, T., He, X. C., Brilke, S., Xiao,
1309 M., Amorim, A., Baalbaki, R., Baccarini, A., Beck, L., Bräkling, S., Murillo, L. C., Chen, D., Chu, B.,
1310 Dada, L., Dias, A., Dommen, J., Duplissy, J., El Haddad, I., Fischer, L., Carracedo, L. G., Heinritzi, M.,
1311 Kim, C., Kim, C., Koenig, T. K., Kong, W., Lamkaddam, H., Lee, C. P., Leiminger, M., Leiminger, M.,
1312 Li, Z., Makhmutov, V., Manninen, H. E., Marie, G., Marten, R., Müller, T., Nie, W., Partoll, E., Petäjä,
1313 T., Pfeifer, J., Philippov, M., Rissanen, M. P., Rissanen, M. P., Rörup, B., Schobesberger, S.,
1314 Schuchmann, S., Shen, J., Sipilä, M., Steiner, G., Stozhkov, Y., Tauber, C., Tham, Y. J., Tomé, A.,
1315 Vazquez-Pufleau, M., Wagner, A. C., Wagner, A. C., Wang, M., Wang, Y., Weber, S. K., Wimmer, D.,
1316 Wimmer, D., Wlasits, P. J., Wu, Y., Ye, Q., Zauner-Wieczorek, M., Baltensperger, U., Carslaw, K. S.,
1317 Curtius, J., Donahue, N. M., Flagan, R. C., Hansel, A., Hansel, A., Kulmala, M., Lelieveld, J., Volkamer,
1318 R., Kirkby, J., Kirkby, J. and Winkler, P. M.: Enhanced growth rate of atmospheric particles from
1319 sulfuric acid, *Atmos. Chem. Phys.*, doi:10.5194/acp-20-7359-2020, 2020.

1320 Suikkanen, S., Laamanen, M. and Huttunen, M.: Long-term changes in summer phytoplankton communities
1321 of the open northern Baltic Sea, *Estuar. Coast. Shelf Sci.*, 71(3–4), 580–592,
1322 doi:10.1016/j.ecss.2006.09.004, 2007.

1323 Suikkanen, S., Pulina, S., Engström-Öst, J., Lehtiniemi, M., Lehtinen, S. and Brutemark, A.: Climate Change
1324 and Eutrophication Induced Shifts in Northern Summer Plankton Communities, *PLoS One*, 8(6), 1–10,
1325 doi:10.1371/journal.pone.0066475, 2013.

1326 SYKE press release (29 August 2019), Summary of algal bloom monitoring June–August 2019: Cyanobacteria
1327 were mostly mixed in the water in the Finnish sea areas, in lakes the cyanobacteria situation varied a lot.
1328 [https://www.syke.fi/enUS/Current/Press_releases/Summary_of_algal_bloom_monitoring_JuneAu\(513](https://www.syke.fi/enUS/Current/Press_releases/Summary_of_algal_bloom_monitoring_JuneAu(513)
1329 [91\)](https://www.syke.fi/enUS/Current/Press_releases/Summary_of_algal_bloom_monitoring_JuneAu(513).

1330 Torn, K., Krause-Jensen, D. and Martin, G.: Present and past depth distribution of bladderwrack (*Fucus*
1331 *vesiculosus*) in the Baltic Sea, *Aquat. Bot.*, 84(1), 53–62, doi:10.1016/j.aquabot.2005.07.011, 2006.

1332 Väkevä, M., Hämeri, K., Puhakka, T., Nilsson, E. D., Hohti, H. and Mäkelä, J. M.: Effects of meteorological
1333 processes on aerosol particle size distribution in an urban background area, *J. Geophys. Res. Atmos.*,
1334 105(D8), 9807–9821, doi:10.1029/1999JD901143, 2000.

1335 Vanhanen, J., Mikkilä, J., Lehtipalo, K., Sipilä, M., Manninen, H. E., Siivola, E., Petäjä, T. and Kulmala, M.:
1336 Particle size magnifier for nano-CN detection, *Aerosol Sci. Technol.*, 45(4), 533–542,
1337 doi:10.1080/02786826.2010.547889, 2011.

1338 Wagner, R., Manninen, H.E., Franchin, A., Lehtipalo, K., Mirme, S., Steiner, G., Petäjä, T., Kulmala,
1339 M.: On the accuracy of ion measurements using a Neutral cluster and Air Ion Spectrometer, *Boreal*
1340 *Environ. Res.*, 21, pp. 230-241, 2016.

1341 Wang, Z., Wu, Z., Yue, D., Shang, D., Guo, S., Sun, J., Ding, A., Wang, L., Jiang, J., Guo, H., Gao, J., Cheung,
1342 H. C., Morawska, L., Keywood, M. and Hu, M.: New particle formation in China: Current knowledge
1343 and further directions, *Sci. Total Environ.*, doi:10.1016/j.scitotenv.2016.10.177, 2017.

1344 Wang, Z. B., Hu, M., Yue, D. L., Zheng, J., Zhang, R. Y., Wiedensohler, A., Wu, Z. J., Nieminen, T. and Boy,
1345 M.: Evaluation on the role of sulfuric acid in the mechanisms of new particle formation for Beijing case,
1346 *Atmos. Chem. Phys.*, 11(24), 12663–12671, doi:10.5194/acp-11-12663-2011, 2011.

1347 Weber, R. J., McMurry, P. H., Mauldin, L., Tanner, D. J., Eisele, F. L., Brechtel, F. J., Kreidenweis, S. M.,
1348 Kok, G. L., Schillawski, R. D. and Baumgardner, B.: A study of new particle formation and growth
1349 involving biogenic and trace gas species measured during ACE 1, *J. Geophys. Res. Atmos.*, 103(D13),
1350 16385–16396, doi:10.1029/97JD02465, 1998.

1351 Weber, R. J., McMurry, P. H., Mauldin, R. L., Tanner, D. J., Eisele, F. L., Clarke, A. D. and Kapustin, V. N.:
1352 New particle formation in the remote troposphere: A comparison of observations at various sites,
1353 *Geophys. Res. Lett.*, 26(3), 307–310, doi:10.1029/1998GL900308, 1999.

1354 Wimmer, D., Buenrostro Mazon, S., Elina Manninen, H., Kangasluoma, J., Franchin, A., Nieminen, T.,
1355 Backman, J., Wang, J., Kuang, C., Krejci, R., Brito, J., Goncalves Morais, F., Turnbull Martin, S.,
1356 Artaxo, P., Kulmala, M., Kerminen, V. M. and Petäjä, T.: Ground-based observation of clusters and
1357 nucleation-mode particles in the Amazon, *Atmos. Chem. Phys.*, 18(17), 13245–13264, doi:10.5194/acp-
1358 18-13245-2018, 2018.

1359 Yan, C., Yin, R., Lu, Y., Dada, L., Yang, D., Fu, Y., Kontkanen, J., Deng, C., Garmash, O., Ruan, J., Baalbaki,
1360 R., Schervish, M., Cai, R., Bloss, M., Chan, T., Chen, T., Chen, Q., Chen, X., Chen, Y., Chu, B.,
1361 Dällenbach, K., Foreback, B., He, X., Heikkinen, L., Jokinen, T., Junninen, H., Kangasluoma, J.,
1362 Kokkonen, T., Kurppa, M., Lehtipalo, K., Li, H., Li, H., Li, X., Liu, Y., Ma, Q., Paasonen, P., Rantala,
1363 P., Pileci, R. E., Rusanen, A., Sarnela, N., Simonen, P., Wang, S., Wang, W., Wang, Y., Xue, M., Yang,
1364 G., Yao, L., Zhou, Y., Kujansuu, J., Petäjä, T., Nie, W., Ma, Y., Ge, M., He, H., Donahue, N. M.,
1365 Worsnop, D. R., Veli-Matti, K., Wang, L., Liu, Y., Zheng, J., Kulmala, M., Jiang, J. and Bianchi, F.:
1366 The Synergistic Role of Sulfuric Acid, Bases, and Oxidized Organics Governing New-Particle
1367 Formation in Beijing, *Geophys. Res. Lett.*, doi:10.1029/2020GL091944, 2021.

1368 Yao, L., Garmash, O., Bianchi, F., Zheng, J., Yan, C., Kontkanen, J., Junninen, H., Mazon, S. B., Ehn, M.,
1369 Paasonen, P., Sipilä, M., Wang, M., Wang, X., Xiao, S., Chen, H., Lu, Y., Zhang, B., Wang, D., Fu, Q.,
1370 Geng, F., Li, L., Wang, H., Qiao, L., Yang, X., Chen, J., Kerminen, V. M., Petäjä, T., Worsnop, D. R.,
1371 Kulmala, M. and Wang, L.: Atmospheric new particle formation from sulfuric acid and amines in a
1372 Chinese megacity, *Science* (80-.), 361(6399), 278–281, doi:10.1126/science.aao4839, 2018.

1373 Yu, H., Ren, L., Huang, X., Xie, M., He, J. and Xiao, H.: Iodine speciation and size distribution in ambient
1374 aerosols at a coastal new particle formation hotspot in China, *Atmos. Chem. Phys.*, doi:10.5194/acp-19-
1375 4025-2019, 2019.

1376 Zhang, R., Wang, L., Khalizov, A. F., Zhao, J., Zheng, J., McGraw, R. L. and Molina, L. T.: Formation of
1377 nanoparticles of blue haze enhanced by anthropogenic pollution, *Proc. Natl. Acad. Sci. U. S. A.*,
1378 106(42), 17650–17654, doi:10.1073/pnas.0910125106, 2009.

1379 Zheng, G., Kuang, C., Uin, J., Watson, T. and Wang, J.: Large contribution of organics to condensational
1380 growth and formation of cloud condensation nuclei (CCN) in the remote marine boundary layer, *Atmos.*

